



Identification of bedrock depth along a downstream segment of Muara Bangkahulu River, Bengkulu City, Indonesia

Lindung Zalbuin Mase¹ · Masyhur Irsyam² · Dian Gustiparani¹ · Annisa Nur Noptapia¹ · Arifan Jaya Syahbana³ · Eko Soebowo³

Received: 19 August 2023 / Accepted: 25 February 2024 / Published online: 4 March 2024
© The Author(s) 2024

Abstract

The downstream area of Muara Bangkahulu River is now becoming one of the developing areas in Bengkulu City. In connection with the limited geological information in the study area, this paper identifies bedrock depth along the river's downstream segment. This study is initiated by collecting site investigation data, including soil profile and ambient noise measurement. The inversion analysis using the Monte Carlo simulated annealing method generates a one-dimensional shear wave velocity profile. The results indicate that areas located near the coastline which are developed as tourism areas are categorised as having high-seismic vulnerability. In contrast, the trading market which is close to the river is categorised as having very high seismic vulnerability. In addition, the study area is categorised as Site Classes C and D. A larger vulnerability level is generally found in areas having low V_{s30} and Site Class D. The results indicate that soft rock or engineering bedrock is identified at a depth of 5 to 91 m depth, medium rock at a depth of 10 to 222 m, and hard at a depth of 40 to 289 m. Information on bedrock depth could be implemented to simulate seismic wave propagation for further study.

Keywords Geological condition · Monte Carlo simulated annealing · Bedrock surface · Shear wave velocity

Introduction

Bengkulu City is known as the capital city of Bengkulu Province, Indonesia. The city is located on the western coast of Sumatra Island. The western coast of Sumatra Island is also known as earthquake-prone in Indonesia (Kurnio et al. 2021). According to the seismotectonic, three primary earthquake sources surround Bengkulu Province, as presented in Fig. 1. Three primary earthquake sources are the Sumatra Subduction, the Mentawai Fault, and the Sumatra Fault. Mase et al. (2021a) mentioned that Bengkulu Province, including the city, has at least experienced shakings from two large earthquakes since the 2000s. Those earthquakes

were known as the M_w 7.9 Bengkulu–Enggano Earthquake in 2000 and the M_w 8.6 Bengkulu–Mentawai Earthquake in 2007. With a magnitude greater than M_w 7, both earthquakes resulted in massive, devastating damage in Bengkulu City (Misliniyati et al. 2018). Even though the situation in Bengkulu City with seismic activity, the development of areas in Bengkulu City shows a promising trend (Mase and Keaw-sawasvong 2022).

One area significantly developing in Bengkulu City is the downstream area of the Muara Bangkahulu River. Putrie et al. (2019) mentioned that the population density in the downstream area of the Muara Bangkahulu increases. The necessity for the area's development to support the population in this area also increases. Therefore, the establishment in this area is also relatively high. Mase et al. (2021b) studied the local site condition and liquefaction potential in the study area. They concluded that the downstream area of Muara Bangkahulu is dominated by Site Classes C and D. It indicates that the study area tends to have relatively medium–high seismic vulnerability. In addition, liquefaction also potential to occur in shallow depths, and the effect of engineering bedrock for seismic ground response analysis is still becoming an issue. In previous studies, the

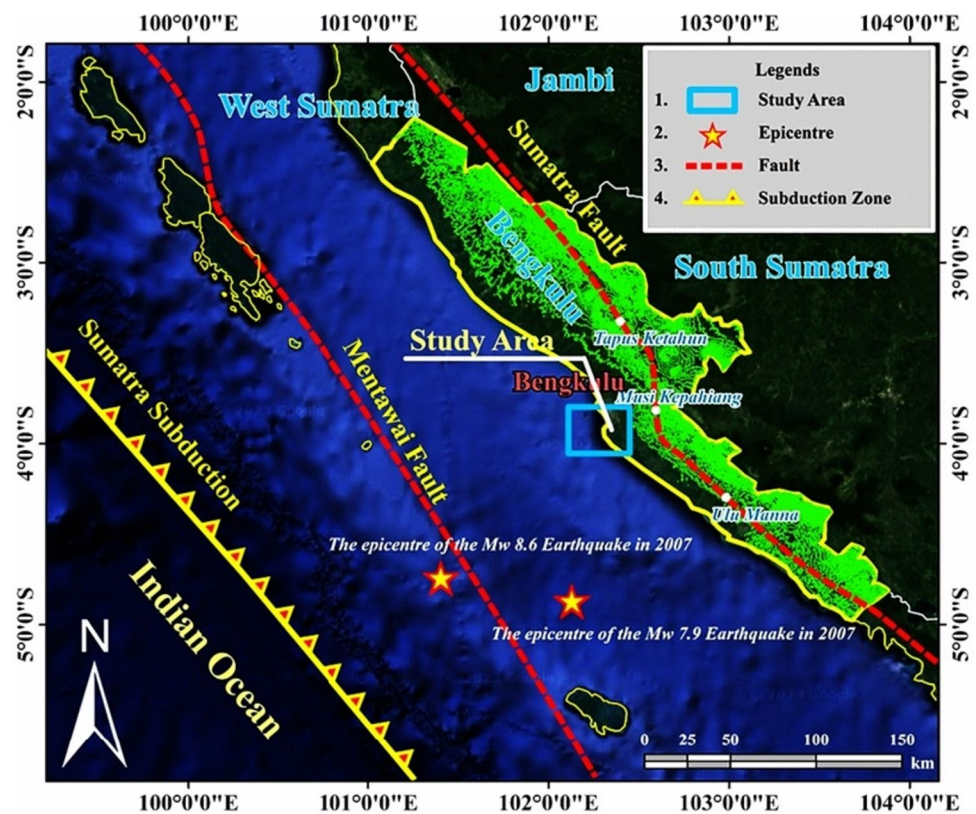
✉ Lindung Zalbuin Mase
lmase@unib.ac.id

¹ Faculty of Engineering, Department of Civil Engineering, University of Bengkulu, Bengkulu 38371, Indonesia

² Faculty of Civil and Environmental Engineering, Department of Civil Engineering, Bandung Institute of Technology, Bandung 40132, Indonesia

³ Research Centre for Geological Disaster, National Research and Innovation Agency, Bandung 40135, Indonesia

Fig. 1 The seismotectonic setting of Bengkulu Province (modified from Mase et al. 2021a)



information related to the bedrock surface in the study area is still limited.

Identifying bedrock depth is essential for spatial development in high-seismic areas (Martorana et al. 2018). Misliniyati et al. (2019) suggested that bedrock identification is essential for seismic ground response analysis. However, the identification of bedrock could be more extensive to implement mechanically. N of 60 blows/ft from standard penetration test (SPT) and cone resistance (q_c) of 250 kg/cm² from cone penetration test (CPT) is generally used to determine a stiff layer. This assumption still needs to be applied in determining the bedrock layer. Miller et al. (1999) introduced shear wave velocity (V_s) as the parameter to identify the bedrock surface. According to Miller et al. (1999), V_s of engineering bedrock should be larger than 760 m/s. For engineering practice, the use of correlation between V_s and site investigation is generally implemented (McGann et al. 2015; Kumar et al. 2022). The empirical analysis from CPT and SPT to estimate V_s from Imai and Tonouchi (1982) exhibits V_s less than 760 m/s for N of 60 blows/ft and (q_c) of 250 kg/cm², in which those values do not represent the bedrock depth.

For some cases on bedrock depth and its implementation such as seismic ground response analysis, the extrapolation method from the bottom of the borehole is employed to estimate the bedrock depth as performed by Mase (2018). It is also not appropriate since unknown geotechnical parameters

from extrapolating depth are unknown. Therefore, the prediction using other methods to estimate bedrock depth should be implemented. From practical implementation, developing empirical equations to estimate bedrock depth based on V_s developed based on SPT and CPT still needs to be significantly improved. In addition, the empirical prediction of bedrock depth based on geophysical parameters could be developed to support other prediction methods, as suggested by Moon et al. (2019) and Manea et al. (2020). V_s profile can be obtained by several methods, such as spectral analysis of surface wave (SASW), multichannel analysis of surface wave (MASW), and inversion analysis for horizontal-vertical spectral ratio (H/V). Generally, the inversion analysis based on an H/V from ambient noise measurement is selected because the method is easy to implement and relatively low-cost.

Several studies of bedrock identification using V_s have been conducted. Moon et al. (2019) conducted a study of bedrock depth evaluation using microtremor measurement in Singapore. Tian et al. (2020) measured small-scale microtremor observation arrays to identify V_s above the fresh bedrock. Farazi et al. (2023) measured ambient noise to obtain a V_s profile to identify the engineering bedrock in the Bengal Basin, Bangladesh. Mase et al. (2023a) studied the geophysical investigation and bedrock identification of the Singaran Pati District, Bengkulu City, Indonesia, using the inversion analysis. Those previous studies generally

stated that implementing bedrock depth using the inversion analysis based on H/V is applicable.

This paper presents the geophysical characteristics, seismic vulnerability, and site seismic resistance. This paper identifies bedrock depth along the Muara Bangkahulu River at the downstream segment. The geophysical exploration using ambient noise measurement is performed in the study area. Furthermore, the inversion technique is implemented to depict the ground profile of the investigated site. The interpolating method is employed to map the bedrock depth. Three bedrock types are soft bedrock (engineering bedrock), medium bedrock, and hard bedrock (seismic bedrock), presented in micro-zonation maps. This study can explain the specific results related to the bedrock surface. The three-dimensional geological models developed based on interpolation mapping are also discussed. In general, the results can also be used in the study area for further analysis, such as seismic ground response analysis. In addition, the results can provide the local government with recommendations for the spatial plan development in the downstream area of the Muara Bangkahulu River.

Geological condition of the study area

Figure 2 presents the geological map of the downstream area of the Muara Bangkahulu River and the position of site investigations which is the studied area in this study. In this study, two main districts crossing the river are investigated. The districts are the Sungai Serut District and the Teluk Segara District. In general, the downstream area of the Muara Bangkahulu River is dominated by two prominent geological formations. The first is Alluvium (Q_a), and the second is Alluvium terraces (Q_{at}). Those formations generally comprise boulders, sands, silts, mud, gravel, and clay materials. According to Sadeghi et al. (2018), the materials composing the sedimented materials from the river stream are generally uncompacted. The liquefaction potential could be high if the materials, such as sandy soils, are under saturated conditions (Sukkarak et al. 2021). In the analysis of seismic ground response along the downstream area of the Muara Bangkahulu River, Mase et al. (2021b) found that the area along the downstream area of the Muara Bangkahulu River could be vulnerable to liquefaction, especially at shallow depths.

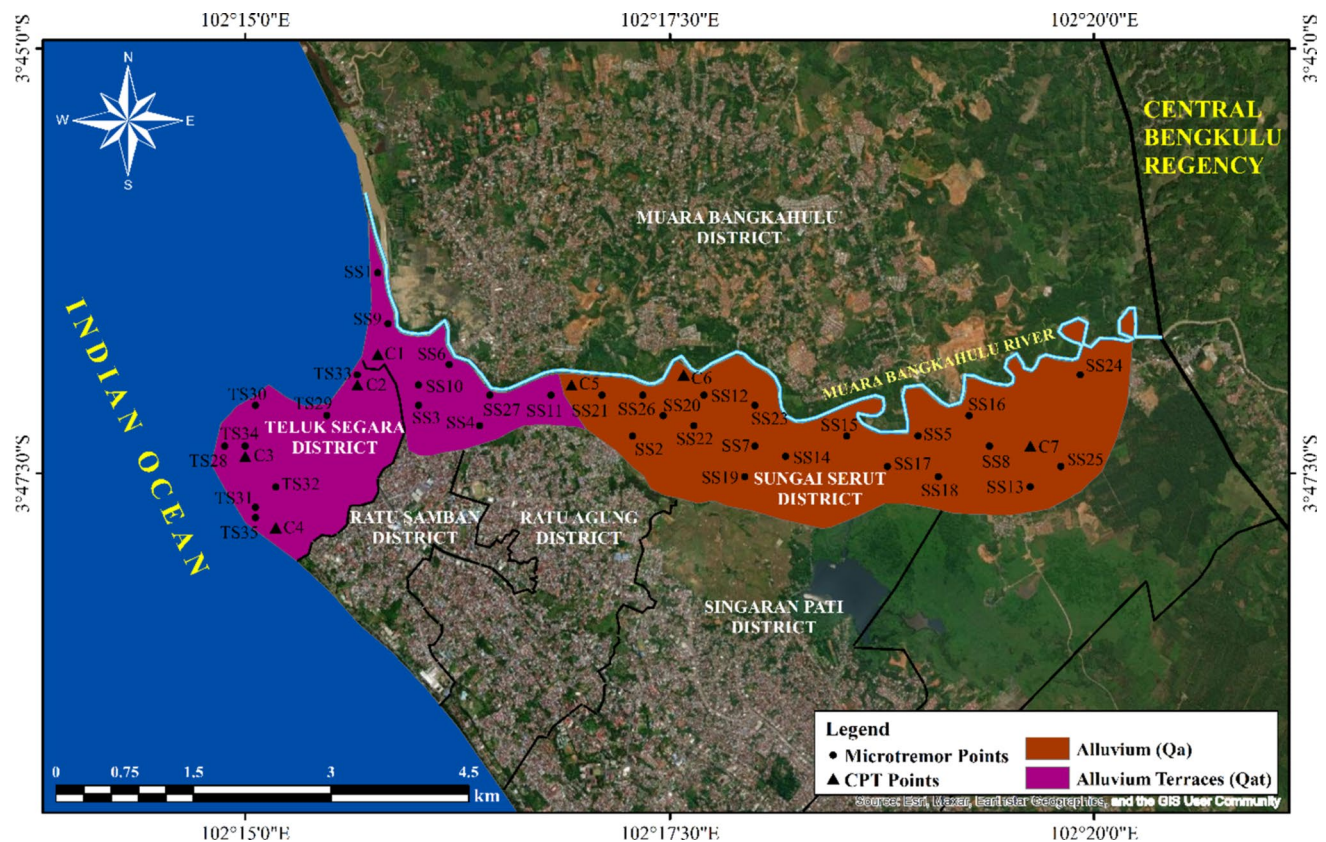


Fig. 2 The geological map and the layout of the site investigation in the study area

Figure 2 also shows the layout of the site investigation in the study area. Figure 2 shows 42 site investigation points, including 35 geophysical measurements and seven cone penetration test (CPT) points conducted. Black circles symbolise ambient noise measurements, and black triangles symbolise CPT points. Notation of TS represents the sites in Teluk Segara District and SS in Sungai Serut. C notation represents CPT test points. Those sites are selected in the study area to depict the geophysical characteristics in the study area. The geophysical measurement uses a seismometer to record the ambient noise of the investigated sites. The ambient noise is then processed to generate a spectral ratio curve. The inversion analysis uses the spectral ratio to generate a one-dimensional ground profile. CPT data is used as the guidelines to define the shallow surface ground in the study area. In CPT points, ambient noise measurement is also performed. It should be noted that CPT tests conducted in this study are addressed to dig the information of subsoil at shallow depths, especially for soil resistance. The CPT tests are used to depict the first three layers for justification in developing a starting guess model. The CPT results are then further analysed to support the starting guess model range composed by several previous studies such as Mase et al. (2021a, 2021b, 2023b) and Misliniyati et al. (2018). Therefore, the use of the supporting data from the CPT test is expected to provide for detailed starting guess model for inversion analysis to result in more accurate results.

Methodology

Ambient noise of microtremor measurement

One of the popular methods to observe geophysical characteristics is the ambient noise of microtremor. This method is also known as the passive method. According to Mirzaoglu and Dykmen (2003), ambient noise (microtremor) is the ground vibration measured using a seismometer sensor. Okada and Suto (2003) mentioned that the ubiquitous, weak, low-amplitude vibrations that may be recorded on the earth's surface are commonly called microtremors. Observations using microtremors assume the shear wave is part of the horizontal motion. Ground vibration generally has a shift amplitude value of 0.1 to 1 micron with the magnitude of the velocity amplitude in the 0.001–0.01 cm/s range. Ground vibration could appear due to several causes, such as the traffic, activity of machine factors, and several activities in construction with the minimum quantity carried out constantly (Kanai 1983).

In the measurement, the ambient noise method assumes that shear wave velocity is a part of the horizontal motion. Several important parameters, such as the natural frequency of the site (f_0) and peak amplitude of horizontal to

vertical spectral ratio (H/V) or A_0 , can be generated. The formulation to determine H/V corresponding to f_0 can be determined based on the following equation (Nakamura 1989),

$$H/V = \sqrt{\frac{H_{(EW)}^2 + H_{(NS)}^2}{2V^2}} \quad (1)$$

H_{EW} and H_{NS} are the Fourier amplitude spectra of horizontal in east–west (EW) and north–south (NS) directions, respectively. V is the Fourier amplitude spectral of vertical.

Nakamura (2008) also suggested that both A_0 and f_0 can be used to estimate the study area's seismic vulnerability index (K_g). The formulation to estimate K_g is expressed in the following equation,

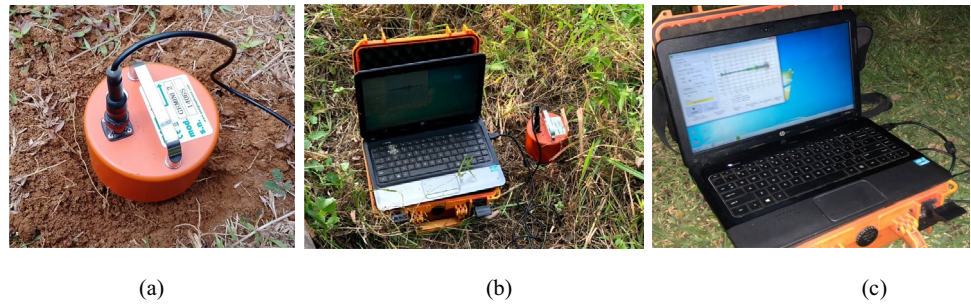
$$K_g = \frac{A^2}{f_0} \quad (2)$$

From Eq. 2, K_g strongly depends on a large A_0 and a smaller f_0 . Akkaya (2020) mentioned that $K_g \leq 3$ indicates low seismic vulnerabilities. The moderate seismic vulnerability level is indicated by $3 < K_g \leq 5$. The moderate seismic vulnerability level is indicated by $5 < K_g \leq 10$. $K_g \geq 10$ indicates a very high seismic vulnerability level.

Several researchers (Lachet et al. 1996; Koçkar and Akgün, 2012; Fat-Helbary et al. 2019) mentioned that ambient noise of the microtremor is applicable for generating the curve of H/V and f_0 . The H/V curve is also applicable to investigate local site conditions. Since the method uses ambient noise as the source, the implementation is relatively sensitive to disturbing effects, such as human activities, environmental settings, and other external actions. Therefore, the measurement should be carefully performed, and the corrections during data processing should be implemented to minimise unnecessary noise.

In this study, a seismometer of PASI Gemini with three acceleration sensors is used to record ambient noise. The three directional directions include east–west (EW), north–south (NS), and up–down (UD) or vertical directions. In practice, the seismometer could measure both weak and strong motions. The on-site measurement is presented in Fig. 3. Figure 3a shows the installation of the seismometer. Installing the seismometer should be performed on soil with a flat surface. Figure 3b shows field measurement, and Fig. 3c shows data processing. In this measurement, the distance between the closest measurement points is 300 to 500 m. In areas with limited access and space for measurements, the distance to the nearest point can range from 500 to 750 m. These considerations are taken to accommodate varying site conditions. With the distribution of site investigation presented in this study, the geophysical characteristics could be well-depicted.

Fig. 3 Measurement process. **a** Installation of seismometer sensor. **b** Setting for measurement mode. **c** Data processing



The measurement is initially by warming the digitisers for about 5 min. This action is taken to reduce low-frequency issues and minimise inappropriate noise for reliable data. A minimum duration of 30 min is implemented in measurement. After measurement, the time series of three microtremor components is divided into time windows of equal or varying length. The window length is inversely proportional to the minimum frequency (Molnar et al 2018). The longer time windows should be used to measure stable low fundamental frequency sites. Fourier spectra were calculated for each time window and smoothed. The ratio between the horizontal and vertical spectrum is then carried out. The data processing is performed from the ambient noise to generate a *H/V* curve. The guidelines from SESAME (2004) for the reliable curve are followed in this study. After determining the reliable curve, a further analysis called the inversion analysis is performed to generate a one-dimensional V_s profile. This study implements an inversion technique based on Monte Carlo sampling simulated annealing proposed by García-Jerez et al. (2016). Several studies conducted by Mase et al. (2020; 2022) and Qodri et al. (2021) showed good model performance.

García-Jerez et al. (2016) suggested that five parameters are required for the analysis of inversion using Monte Carlo sampling annealing. Those parameters are the shear wave velocity (V_s) (in m/s), the pressure wave velocity (V_p) (in m/s), the thickness of the soil layer (h) (in m), the density of soil (ρ) (in kg/m^3), and the ratio of Poisson (ν) (no unit). Monte Carlo simulation is performed for each parameter with minimum to maximum ranges. Wathelet (2008) suggested that for the inversion analysis, a priori knowledge of geological conditions should be determined to minimise the uncertainty during the simulation. In this study, the role of site investigation data and geological conditions is essential to expect a priori knowledge of subsoil properties in the study area. The parameters are generally interdependent for some parameters, such as V_s , V_p , and Poisson’s ratio. Salencon (2001) suggested that those parameters can be correlated based on elastic theory. The analysis is started

Table 1 The distribution of starting guess model-based soil profiles for the inversion analysis

Guidelines models	Sites
Profile 1 (Table 2)	C1, SS9, SS6, SS4
Profile 2 (Table 3)	C2, SS10, SS1, SS3, TS29, TS25
Profile 3 (Table 4)	C3, TS23, TS30, TS26
Profile 4 (Table 5)	C4, TS27, TS31, TS28
Profile 5 (Table 6)	C5, SS11, SS21
Profile 6 (Table 7)	C6, SS20, SS2, SS12, SS22, SS23, SS19, SS14
Profile 7 (Table 8)	C7, SS16, SS8, SS5, SS15, SS17, SS18, SS13, SS24, SS25

by searching the initial guess model, whose parameters are randomly selected within the range of soil properties. The inversion analysis is conducted based on the range of soil properties suggested in Table 1, 2, 3, 4, 5, 6, 7 and 8. The starting guess model profiles are presented in Fig. 4. The starting guess model ranges are considered based on previous studies conducted by Mase et al. (2021a and 2021b) and Misliniyati et al. (2018).

The inversion analysis is conducted until the *H/V* curve from measurement is generally consistent with the *H/V* curve from inversion. Herak (2008) suggested that the misfit of inversion should be implemented to assess the reliability of inversion results, as presented in the following equations,

$$m = \sum_i \{ [H/V_{\text{measurement}}(f_i) - H/V_{\text{inversion}}(f_i)] W_i \}^2 \tag{3}$$

$$W_i = [H/V_{\text{measurement}}(f_i)]^E \tag{4}$$

$$E \geq 0 \tag{5}$$

where, $H/V_{\text{measurement}}$ is the measured *H/V* and $H/V_{\text{inversion}}$ is *H/V* from the inversion analysis. W_i is the weight factor defined by Eq. 3. Depending on W_i , larger weights (for $E > 0$) are given to data around the frequencies where the observed HVSr is large.

Table 2 General range values of initial parameters for H/V inversion for C1, SS9, SS4, and SS6

Layer	Soil type (USCS)	Thickness (m)	V_s (m/s)	V_p (m/s)	Density (ρ) kg/m ³	Poisson's ratio (ν)
Layer 1	Clay (OH, OL, CL, CH)	0–15	100–400	300–500	1800–2100	0.400–0.495
Layer 2	Sand (SP, SM, SC)	0–15	200–500	400–600	1800–2100	0.200–0.400
Layer 3	Sand (SP, SM, SC)	0–15	225–600	400–700	1800–2100	0.200–0.400
Layer 4	Sand (SP, SM, SC)	0–15	300–600	400–800	1800–2100	0.200–0.400
Layer 5	Soft rock	0–50	760–1080	950–1350	2000–2300	0.100–0.200
Layer 6	Medium rock	0–50	1080–2000	1350–2500	2000–2300	0.100–0.200
Layer 7	Hard rock	~	2000–3000	2500–4000	2000–2300	0.100–0.200

Table 3 General range values of initial parameters for H/V inversion for C2, SS10, SS1, SS3, TS29, and TS25

Layer	Soil type (USCS)	Thickness (m)	V_s (m/s)	V_p (m/s)	Density (ρ) kg/m ³	Poisson's ratio (ν)
Layer 1	Clay (OH, OL, CL, CH)	0–15	100–400	300–500	1800–2100	0.400–0.495
Layer 2	Clay (OH, OL, CL, CH)	0–15	200–500	400–600	1800–2100	0.400–0.495
Layer 3	Sand (SP, SM, SC)	0–15	225–600	400–800	1800–2100	0.200–0.400
Layer 4	Sand (SP, SM, SC)	0–15	300–700	400–800	1800–2100	0.200–0.400
Layer 5	Sand (SP, SM, SC)	0–30	400–760	500–940	1800–2100	0.200–0.400
Layer 6	Soft rock	0–50	760–1080	950–1350	2000–2300	0.100–0.200
Layer 7	Medium rock	0–50	1080–2000	1350–2500	2000–2300	0.100–0.200
Layer 8	Hard rock	~	2000–3000	2500–4000	2000–2300	0.100–0.200

Table 4 General range values of initial parameters for H/V inversion for C3, TS23, TS30, and TS26

Layer	Soil type (USCS)	Thickness (m)	V_s (m/s)	V_p (m/s)	Density (ρ) kg/m ³	Poisson's ratio (ν)
Layer 1	Clay (OH, OL, CL, CH)	0–15	80–300	100–350	1800–2100	0.400–0.495
Layer 2	Clay (OH, OL, CL, CH)	0–15	100–400	125–600	1800–2100	0.400–0.495
Layer 3	Clay (OH, OL, CL, CH)	0–15	150–500	180–625	1800–2100	0.400–0.495
Layer 4	Clay (OH, OL, CL, CH)	0–15	200–600	400–800	1800–2100	0.200–0.400
Layer 5	Sand (SP, SM, SC)	0–15	250–700	425–900	1800–2100	0.200–0.400
Layer 6	Sand (SP, SM, SC)	0–80	300–725	500–940	1800–2100	0.200–0.400
Layer 7	Soft rock	0–150	760–1080	950–1350	2000–2300	0.100–0.200
Layer 8	Medium rock	0–150	1080–2000	1350–2500	2000–2300	0.100–0.200
Layer 9	Hard rock	~	2000–3000	2500–4000	2000–2300	0.100–0.200

Table 5 General range values of initial parameters for H/V inversion for C4, TS27, TS31, TS28

Layer	Soil type (USCS)	Thickness (m)	V_s (m/s)	V_p (m/s)	Density (ρ) kg/m ³	Poisson's ratio (ν)
Layer 1	Clay (OH, OL, CL, CH)	0–15	100–300	100–400	1700–2100	0.400–0.495
Layer 2	Clay (OH, OL, CL, CH)	0–15	150–400	200–500	1700–2100	0.400–0.495
Layer 3	Sand (SP, SM, SC)	0–15	200–500	225–600	1800–2100	0.200–0.400
Layer 4	Sand (SP, SM, SC)	0–15	250–600	300–700	1800–2100	0.200–0.400
Layer 5	Sand (SP, SM, SC)	0–30	280–760	325–900	1800–2100	0.200–0.400
Layer 6	Soft rock	0–50	760–1080	950–1350	2000–2300	0.100–0.200
Layer 7	Medium rock	0–50	1080–2000	1350–2500	2000–2300	0.100–0.200
Layer 8	Hard rock	~	2000–3000	2500–4000	2000–2300	0.100–0.200

Table 6 General range values of initial parameters for H/V inversion for C5, SS11, and SS21

Layer	Soil type (USCS)	Thickness (m)	V_s (m/s)	V_p (m/s)	Density (ρ) kg/m ³	Poisson's ratio (ν)
Layer 1	Clay (OH, OL, CL, CH)	0–10	100–400	100–350	1700–2100	0.400–0.495
Layer 2	Clay (OH, OL, CL, CH)	0–10	200–425	150–500	1700–2100	0.400–0.495
Layer 3	Clay (OH, OL, CL, CH)	0–10	225–450	200–525	1700–2100	0.400–0.495
Layer 4	Sand (SP, SM, SC)	0–10	250–525	250–650	1800–2100	0.200–0.400
Layer 5	Clay (OH, OL, CL, CH)	0–10	275–550	300–675	1700–2100	0.400–0.495
Layer 6	Clay (OH, OL, CL, CH)	0–10	275–600	325–700	1700–2100	0.400–0.495
Layer 7	Sand (SP, SM, SC)	0–10	275–625	350–725	1800–2100	0.200–0.400
Layer 8	Clay (OH, OL, CL, CH)	0–10	300–700	400–750	1700–2100	0.400–0.495
Layer 9	Clay (OH, OL, CL, CH)	0–15	400–725	425–800	1700–2100	0.400–0.495
Layer 10	Clay (OH, OL, CL, CH)	0–15	400–750	500–1000	1700–2100	0.400–0.495
Layer 11	Sand (SP, SM, SC)	0–30	450–760	525–1020	1800–2100	0.200–0.400
Layer 12	Soft rock	0 – 100	760–1080	950–1350	2000–2300	0.100–0.200
Layer 13	Medium rock	0–120	1080–2000	1350–2500	2000–2300	0.100–0.200
Layer 14	Hard rock	~	2000–3000	2500–4000	2000–2300	0.100–0.200

Table 7 General range values of initial parameters for H/V inversion for C6, SS20, SS2, SS12, SS22, SS23, SS19, and SS14

Layer	Soil type (USCS)	Thickness (m)	V_s (m/s)	V_p (m/s)	Density (ρ) kg/m ³	Poisson's ratio (ν)
Layer 1	Clay (OH, OL, CL, CH)	0–10	100–400	100–350	1700–2200	0.400–0.495
Layer 2	Clay (OH, OL, CL, CH)	0–10	200–425	150–500	1700–2200	0.400–0.495
Layer 3	Sand (SP, SM, SC)	0–10	225–450	200–525	1800–2200	0.200–0.400
Layer 4	Clay (OH, OL, CL, CH)	0–10	250–525	250–650	1700–2200	0.400–0.495
Layer 5	Sand (SP, SM, SC)	0–10	275–550	300–675	1800–2200	0.200–0.400
Layer 6	Clay (OH, OL, CL, CH)	0–10	275–600	325–700	1700–2200	0.400–0.495
Layer 7	Clay (OH, OL, CL, CH)	0–10	275–625	350–725	1700–2200	0.400–0.495
Layer 8	Clay (OH, OL, CL, CH)	0–10	300–700	400–750	1700–2200	0.400–0.495
Layer 9	Sand (SP, SM, SC)	0–15	400–725	425–800	1800–2200	0.200–0.400
Layer 10	Clay (OH, OL, CL, CH)	0–15	400–750	500–1000	1700–2300	0.400–0.495
Layer 11	Sand (SP, SM, SC)	0–30	450–760	525–1020	2000–2300	0.200–0.400
Layer 12	Soft rock	0–100	760–1080	950–1350	2000–2300	0.100–0.200
Layer 13	Medium rock	0–130	1080–2000	1350–2500	2000–2300	0.100–0.200
Layer 14	Hard rock	~	2000–3000	2500–4000	2000–2300	0.100–0.200

Table 8 General range values of initial parameters for H/V inversion for C7, SS16, SS8, SS5, SS15, SS17, SS18, SS13, SS24, and SS25

Layer	Soil type (USCS)	Thickness (m)	V_s (m/s)	V_p (m/s)	Density (ρ) kg/m ³	Poisson's ratio (ν)
Layer 1	Clay (OH, OL, CL, CH)	0–15	100–400	100–450	1700–2200	0.400–0.495
Layer 2	Clay (OH, OL, CL, CH)	0–15	200–450	300–600	1700–2200	0.400–0.495
Layer 3	Sand (SP, SM, SC)	0–15	250–500	350–625	1800–2200	0.200–0.400
Layer 4	Clay (OH, OL, CL, CH)	0–15	275–550	400–700	1700–2200	0.400–0.495
Layer 5	Sand (SP, SM, SC)	0–15	300–600	450–725	1800–2200	0.200–0.400
Layer 6	Clay (OH, OL, CL, CH)	0–15	300–650	500–750	1700–2200	0.400–0.495
Layer 7	Sand (SP, SM, SC)	0–15	425–700	525–775	1800–2200	0.200–0.400
Layer 8	Sand (SP, SM, SC)	0–30	550–760	600–900	2000–2300	0.200–0.400
Layer 9	Soft rock	0–50	760–1080	950–1350	2000–2300	0.100–0.200
Layer 10	Medium rock	0–50	1080–2000	1350–2500	2000–2300	0.100–0.200
Layer 11	Hard rock	~	2000–3000	2500–4000	2000–2300	0.100–0.200

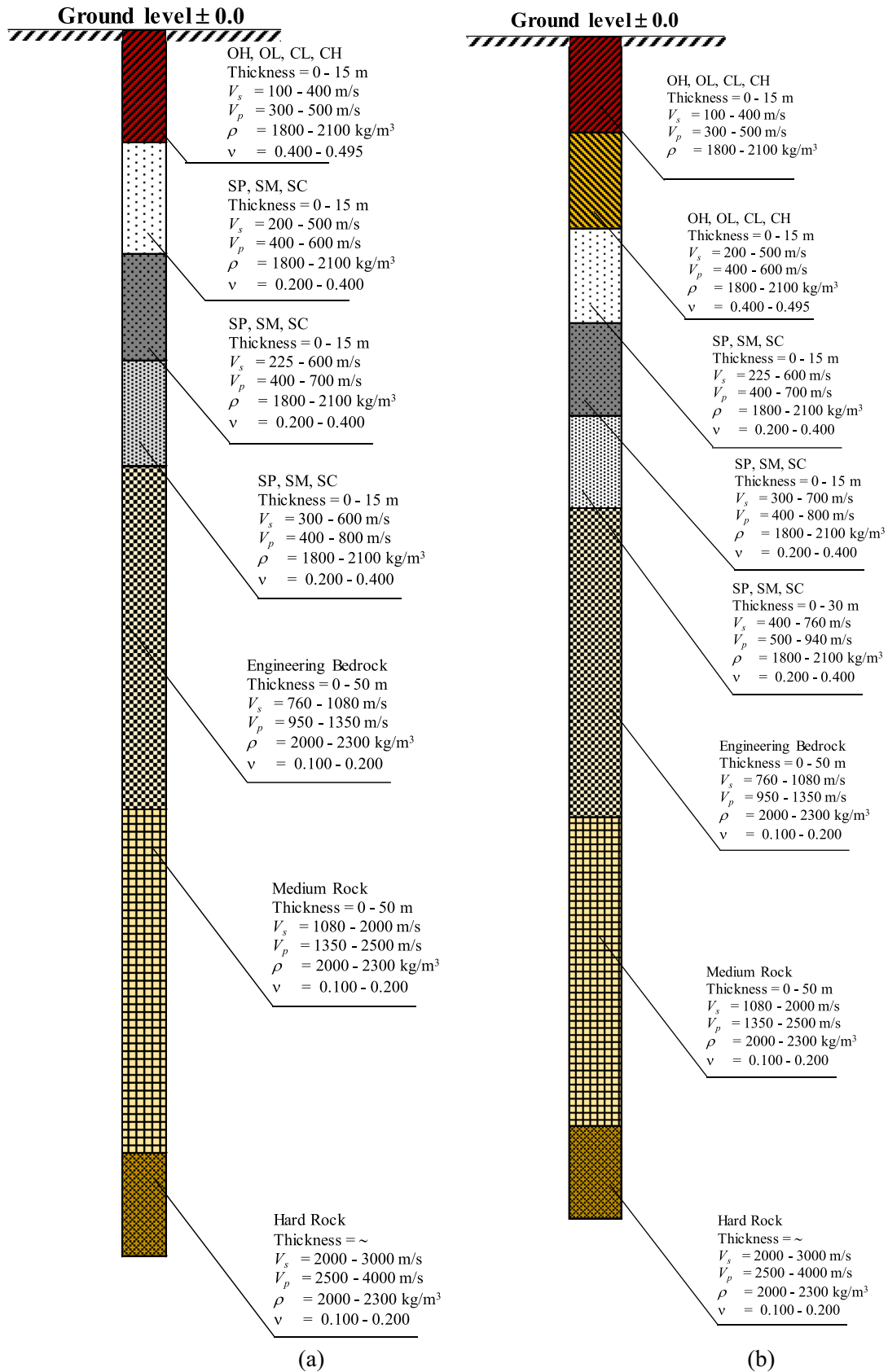


Fig. 4 Typical boring-log profiles for starting guess model based on Table 2 (a), Table 3 (b), Table 4 (c), Table 5 (d), Table 6 (e), Table 7 (f), and Table 8 (g)

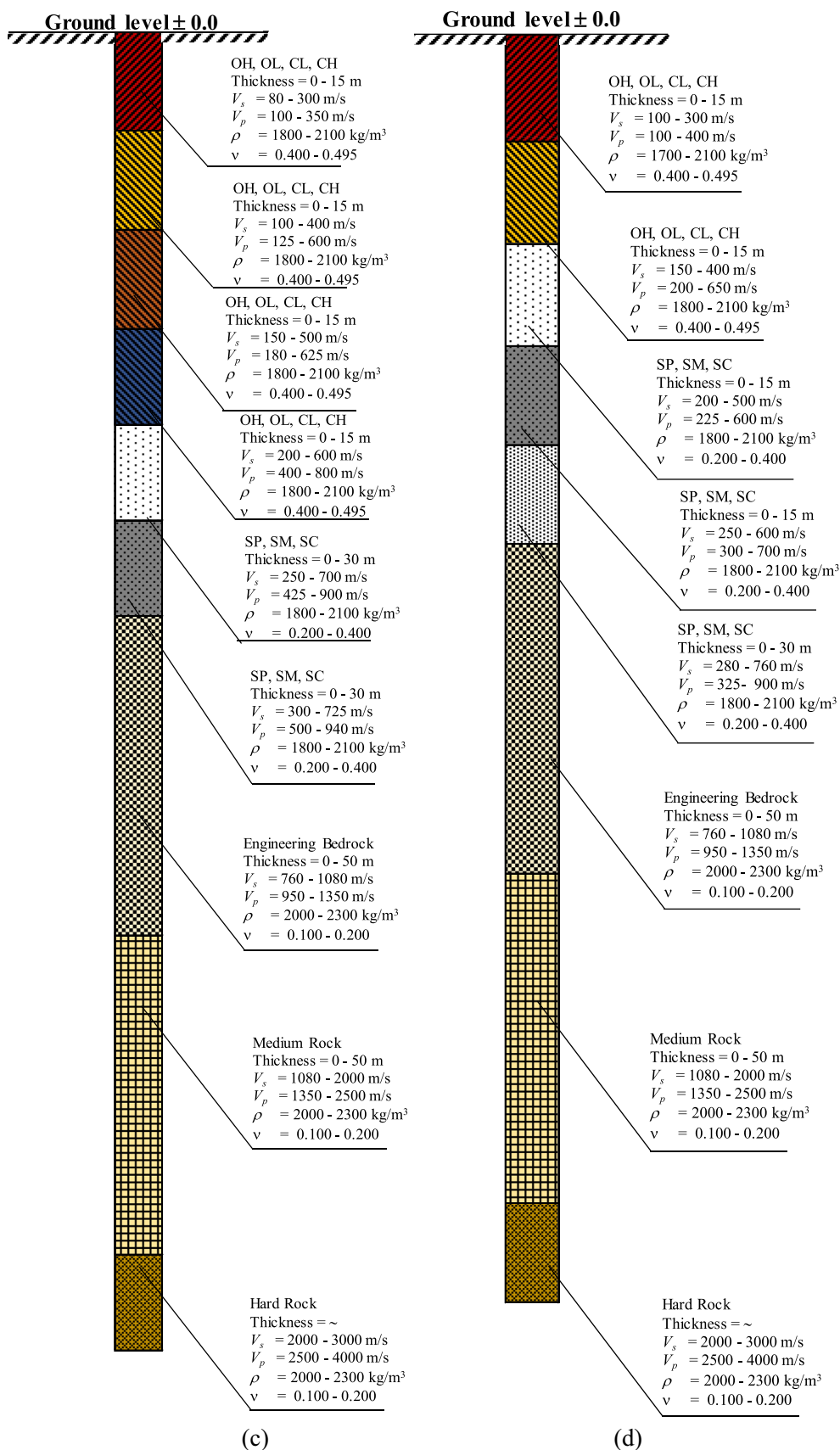


Fig. 4 (continued)

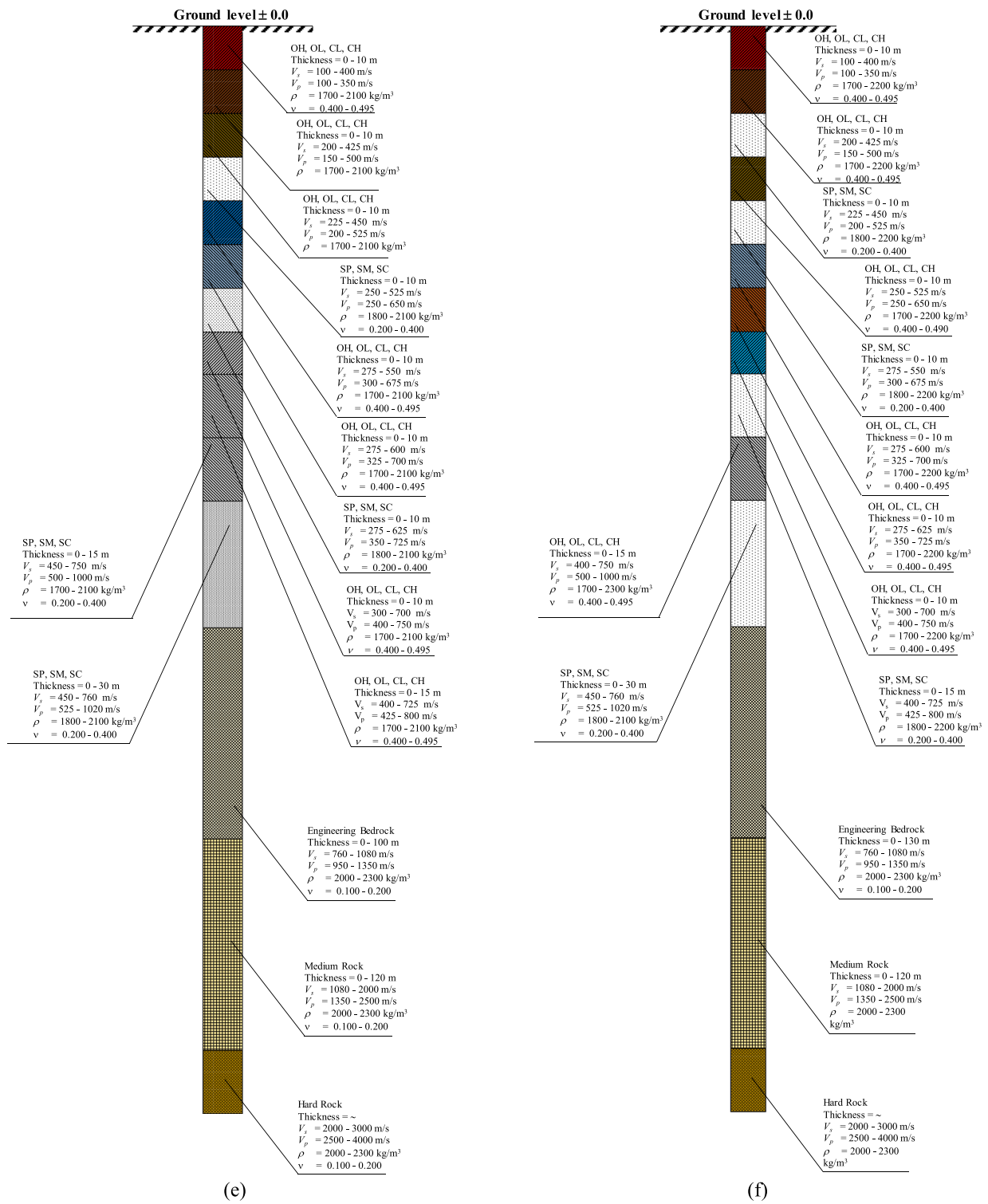


Fig. 4 (continued)

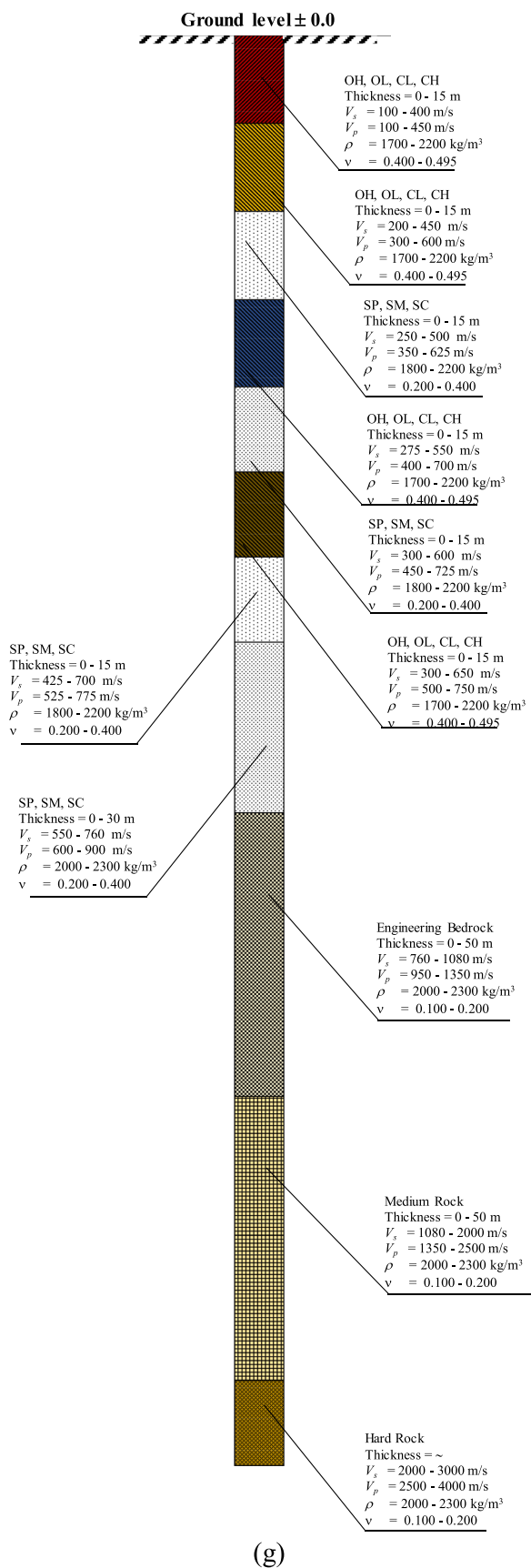


Fig. 4 (continued)

Site and bedrock classifications

A parameter called the time-averaged shear wave velocity for the first 30 m depth (V_{s30}) is applicable to define site characteristics. The parameter is estimated based on the following equation,

$$V_{s30} = \frac{30}{\sum_{i=1}^n \frac{d_i}{V_i}} \tag{6}$$

where d_i is the thickness of each layer, V_{si} is the shear wave velocity in each layer, and n is the number of layers.

According to the National Earthquake Hazard Reduction Program or NEHRP (1998), site classification can be divided into six classes, as presented in Table 9. In Table 9, the site classifications are Class A, Class B, Class C, Class D, Class E, and Class F. Classes A and B indicate the rock site, whereas Classes C, D, and E indicate the soil site. The information on site class is also included as a parameter for the ground motion prediction equation implemented in Next Generation Attenuation (NGA) models (Tanapalungkorn et al. 2020; Ahdi et al. 2022). Class A is for sites with V_{s30} more than 1500 m/s, whereas Class B is for sites with V_{s30} ranging from 760 to 1500 m/s, and V_{s30} for Class C ranges from 360 to 760 m/s; Class D, 180 to 360 m/s; Class E, less than 180 m/s. Class F is destined for a site requiring specific treatment, such as a liquefiable layer.

Pinzon et al. (2019) suggested that V_s values from geophysical measurements can be used to determine the bedrock depth. Miller et al. (1999) mentioned that V_s of 760 can be used as the minimum criteria for engineering bedrock or soft rock. Therefore, the minimum V_s or 1500 m/s could be assigned as a medium rock. A minimum V_s of 2000 m/s could be used for seismic bedrock or hard rock.

Research framework

The research framework for this study is presented in Fig. 5. First, this study is initiated by problem definition. The question of the depth of engineering bedrock and the need to understand the depth of engineering bedrock for seismic ground response analysis is the issue researchers would like to address in this study. Next, the site investigation is conducted to observe the site condition of the study area. The microtremor's ambient noise is measured using a seismometer to generate the H/V curve. The H/V curve is assessed based on the criteria of reliable peak suggested by SESAME (2004). Afterwards, the inversion analysis is performed by referring to the starting guess model shown in Tables 2, 3, 4, 5, 6, 7 and 8. The inversion analysis is performed until the H/V curve from inversion is generally consistent with the

Table 9 Soil classification based on the value of shear wave velocity at a depth of 30 m (V_{s30}) (NEHRP 1998)

A	Hard rock	$V_{s30} > 1500$
B	Rock	$760 < V_{s30} \leq 1500$
C	Very dense soil and soft rock	$360 < V_{s30} \leq 760$
D	Stiff soil ($15 \leq N \leq 50$ or $50 \text{ kPa} \leq s_u \leq 100 \text{ kPa}$)	$180 < V_{s30} \leq 360$
E	Soft soil or any profile with more than 3 m soft clay defined as soil	$V_{s30} \leq 180$
F	with $PI > 20$, $w \geq 40\%$, and $s_u < 25 \text{ kPa}$ Soils requiring site-specific evaluations	

N , SPT (blows/ft); s_u , undrained shear strength (kPa); PI , Plasticity index; w , water content (%)

H/V curve from measurement. The inversion method from García-Jerez et al. (2016) is implemented in this study.

The measurement results, such as amplification and predominant frequency in each investigated site, are presented in micro zonation maps. Several representative sites are presented and discussed in this study. The best model for matched H/V curve from inversion is then generated. A one-dimensional V_s profile is generated for each investigated site. In addition, parameters such as V_p and unit weight are also interpreted in the ground profile. Furthermore, V_{s30} and site classification based on NEHRP (1998) are analysed. V_{s30} and Site Class maps are also presented in this study. The inversion analysis is performed to reach the bedrock information. Therefore, three bedrock depths, i.e. engineering bedrock, medium rock, and hard rock depths, are also interpreted into micro zonation maps. In general, the results of this study could provide information on geophysical characteristics in the study area. The information on bedrock depth from the study area could be used for further analysis, such as ground response analysis.

Results and discussions

Amplification, predominant frequency, seismic vulnerability distributions

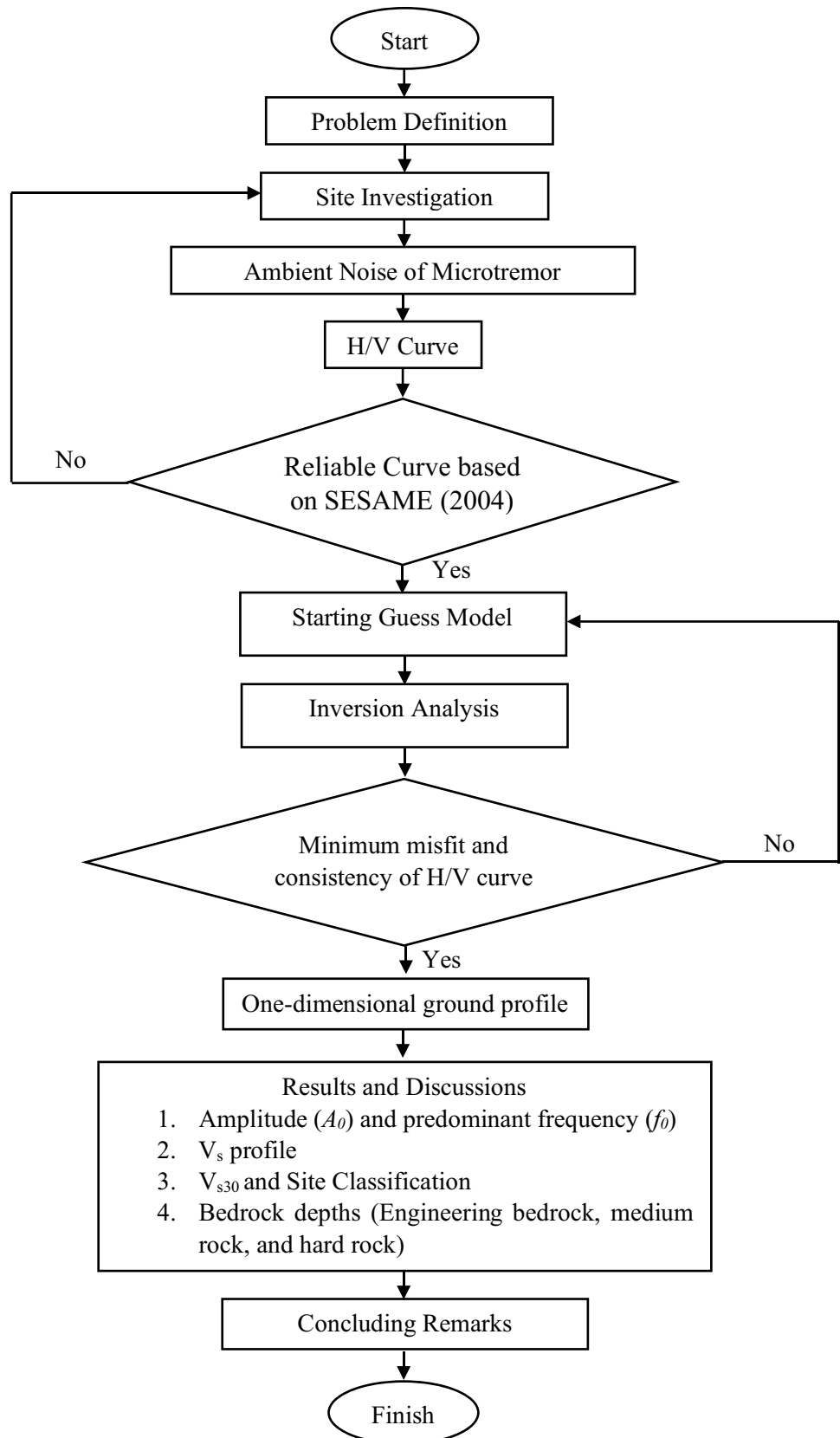
Figure 6 presents the distribution map of amplification (A_0) in the study area. Based on the figure, it can be observed that there are two dominant amplification ranges in the study area. The first is amplification less than 3 Hz (purple colour), and the second is amplification ranging from 3 to 5.5 (green colour). There are also several ranges of amplification, i.e. 5.5 to 8 (yellow colour), 8 to 10.5 (orange colour), and 8.0 to 12.5 (red colour). The maximum amplification (red colour) is generally concentrated in the western part of the study area. The minimum amplification (purple colour) is generally concentrated in the middle of the study area. In the western part, Gosar (2017) suggested that a larger impedance contrast between rock and sediment could happen in the site having a large amplification. A large amplification simply indicates that bedrock is harder and less fractured (Baize

et al. 2016). As shown in Fig. 5, It can be observed that the further west, the greater the amplification value. Therefore, the bedrock in the western study area could be harder and located at a shallow depth.

Figure 7 presents the distribution map of predominant frequency (f_0) in the study area. As presented in Fig. 7, it can be observed that there are also two main dominant ranges of f_0 in the study area. The first one is f_0 ranging from 0 to 3 Hz, and the second is f_0 ranging from 3 to 7 Hz. The small parts for frequencies ranging from 7 to 11 Hz and 11 to 16 Hz are also found in the eastern part of the study area. The small part with a high frequency located in the eastern part area indicates the thin sediment thickness. The amplification in this small part zone is also relatively small. It means that the impedance contrast between rock and sediment is relatively low. It could be caused by the soil layers in this zone tend to have a high soil resistance. According to a study conducted by Mase et al. (2021b), the soil resistance in this zone is high. Based on the liquefaction site response analysis conducted by Mase et al. (2021b), the liquefaction potential and earthquake damage are relatively low. It indicates that geophysical and geotechnical characteristics in this zone are quite different from other neighbouring sites. In the western part of the study area, the further west, the greater the predominant frequency value. Mase et al. (2021a) and Putti and Satyam (2020) mentioned that an area with a lower predominant frequency indicates a thicker sediment thickness. Otherwise, Stanko and Markušić (2020) suggested that a site with high predominant frequency indicates a thin sediment thickness over the bedrock. It also indicates the shallow bedrock depth.

In line with the amplification and predominant frequency presented in Figs. 6 and 7, the seismic vulnerability based on those parameters can be depicted. Figure 8 presents the distribution map of the study area's seismic vulnerability index or K_g . In general, the study area tends to have a low seismic vulnerability level, especially in the middle part of the study area. Moderate seismic vulnerability level is generally found in the western and eastern parts of the study area. Akkaya (2020) suggested that combining significant amplification and low predominant frequency values could indicate high seismic vulnerability. Significant amplification and low predominant frequency are generally found in the

Fig. 5 Research flowchart



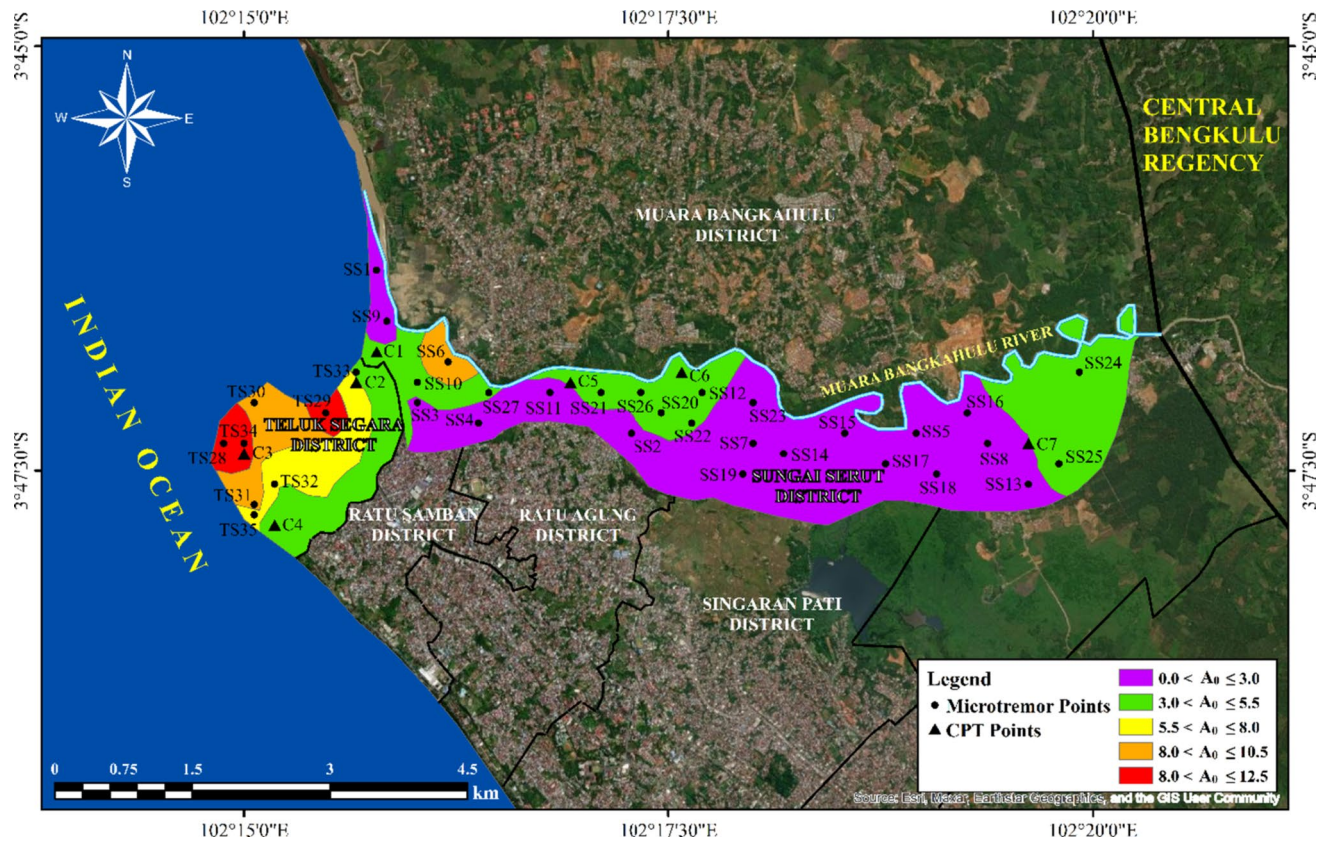


Fig. 6 Distribution map of amplification (A_0) in the study area

western and northern parts of the study area. The high to very high seismic vulnerability level is generally concentrated in the eastern and western parts of the study area. A study on seismic damage during the major earthquakes in Bengkulu City has been performed. Mase et al. (2023c) suggested that during the M_w 8.6 Bengkulu–Mentawai Earthquake in 2007, the damage intensity level in the study area is about Scale VIII to IX in MMI. The damage intensity level could reach Scale IX in MMI for the western, eastern, and northern parts. Therefore, in line with the findings in this study, it can be predicted that seismic damage could be more significant in these areas.

The velocity profiles

Figure 9 compares the H/V curves obtained from measurement and inversion. In Fig. 8, four sites are selected as representative sites. SS1 represents the estuary area of Muara Bangkahulu River (Fig. 8a), SS20 represents the trading market area (Fig. 8b), SS24 represents the housing area (Fig. 8c), and TS35 represents the coastal tourist area (Fig. 8d). In general, it can be observed that A_0 values for representative sites range from 2.64 to 5.42. For the frequency, the values range from 2.29 to 5.38 Hz. These values

are generally consistent with amplification and frequency maps in Figs. 5 and 6. In terms of the inversion analysis, it can be observed that the inversion curve is generally consistent with the measurement curve. It indicates that the ground profile model from inversion analysis is relatively in line with the actual condition in the study area.

The inversion analysis can generate the best model of the ground profile. Figure 10 presents the velocity and ground profile models obtained from the inversion analysis. For SS1 (Fig. 10a), it can be observed that sandy soils generally dominate soil layers. V_{s30} in SS1 is about 293.78 m/s. According to NEHRP (1998), SS1 has been categorised as Site Class D. The depth of engineering bedrock is predicted at 52.3 m, whereas the medium rock is found at 56.0 m. The surface is found at a depth of 65.9 m for hard rock.

For SS20 (Fig. 10b), the variation of the soil layer is generally significant compared to SS1. Clay and sand layers generally dominate up to 60.3 m below the ground surface. V_{s30} of SS20 is 325.01 m/s which indicates Site Class D. In SS20, engineering bedrock, medium rock, and hard rock surfaces can be found at depths of 60.3-, 158.4-, and 257.4-m below ground surface, respectively.

Figure 10c presents the velocity and ground profiles for SS24. The soil variations for this site are also significant.

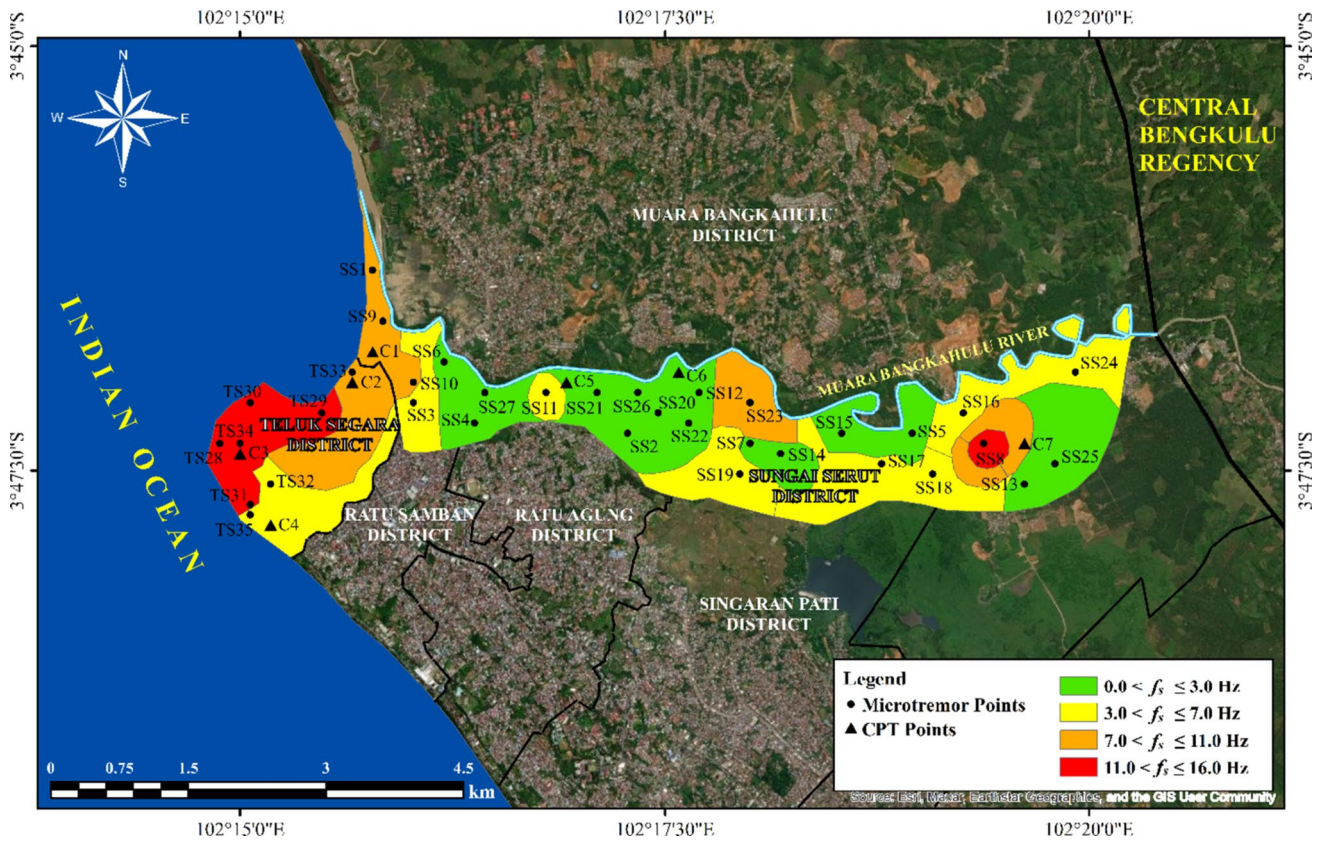


Fig. 7 Distribution map of frequency (f_b) in the study area

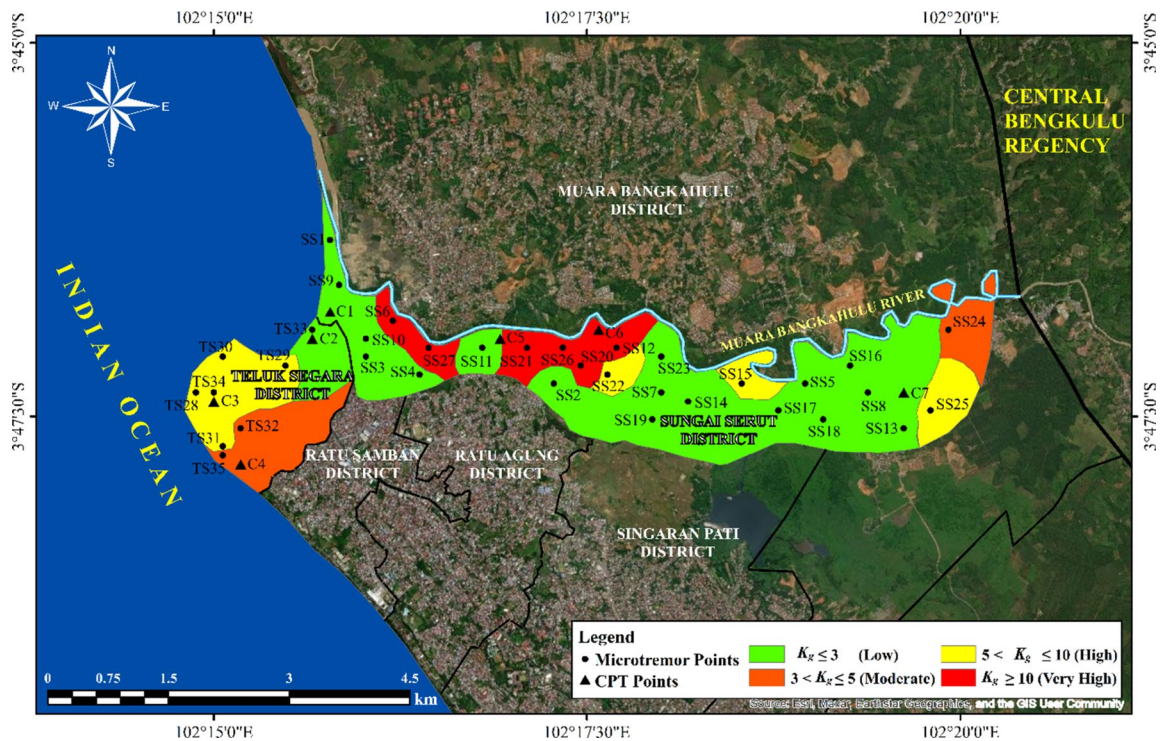


Fig. 8 Distribution map of seismic vulnerability index (K_g) in the study area

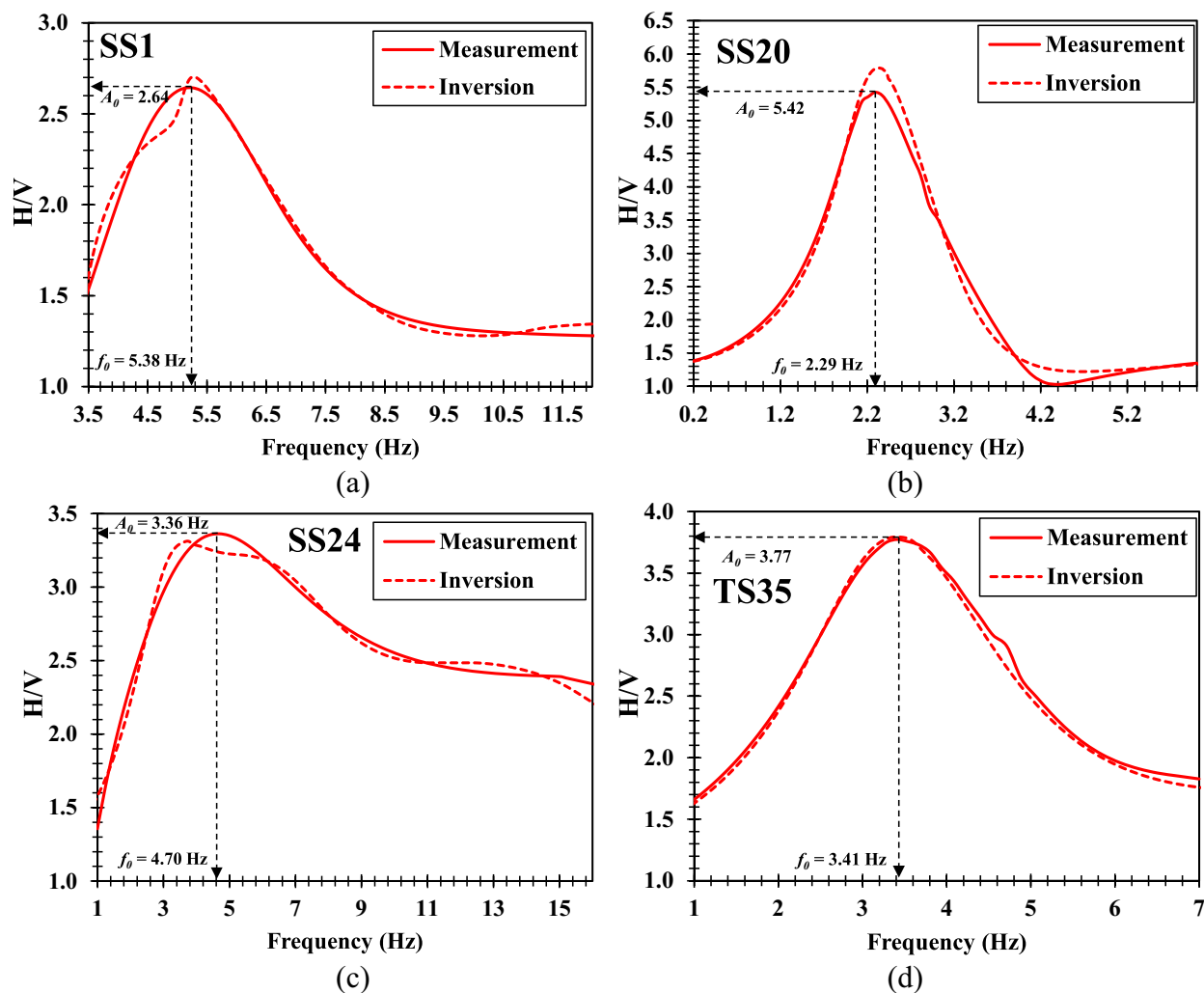


Fig. 9 The H/V curve comparisons between measurement and inversion for sites SS1 (a), SS20 (b), SS24 (c), and TS35 (d)

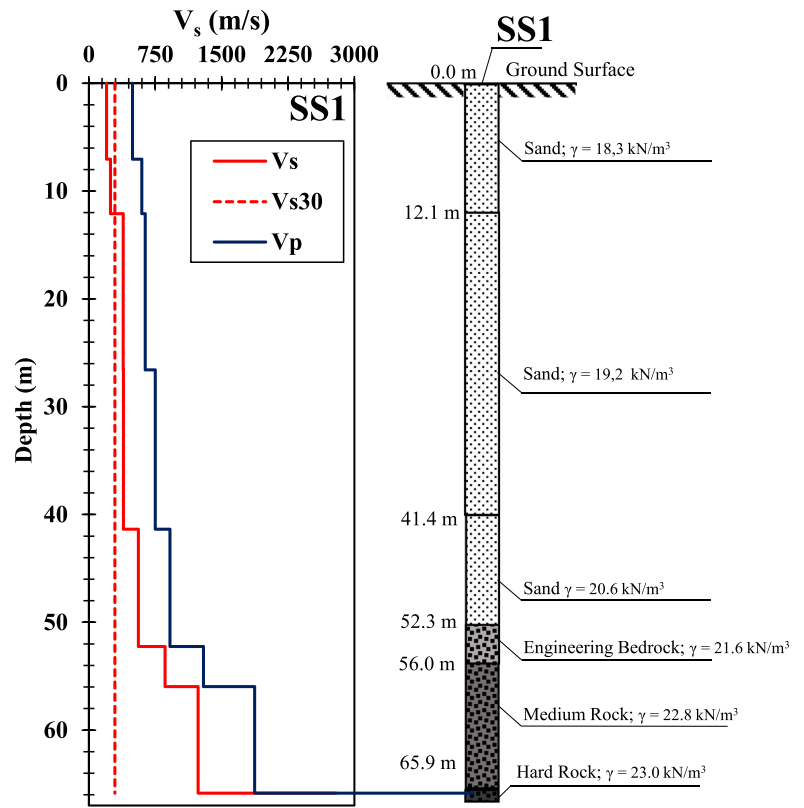
Several thin clay layers are also found on the site, which is underlain by a sand layer. V_{s30} of SS24 is about 465.53 m/s; therefore, the site is categorised as Site Class C. The engineering bedrock in SS24 is found at a depth of 19.9 m, whereas medium rock is found at 42.4 m. Hard rock is found at a depth of 89.5 m.

Figure 10d presents the velocity and ground profiles in Site TS35. The site is categorised as Site Class C because V_{s30} of this site is 453.35 m/s. Sand layers dominate TS35 because the site is located near the coastal area of Bengkulu City. Based on the inversion analysis, it can be observed that engineering bedrock is generally found at a depth of 25.4 m, and medium bedrock is found at a depth of 47.2 m/s. Hard rock is found at a depth of 96.7 m.

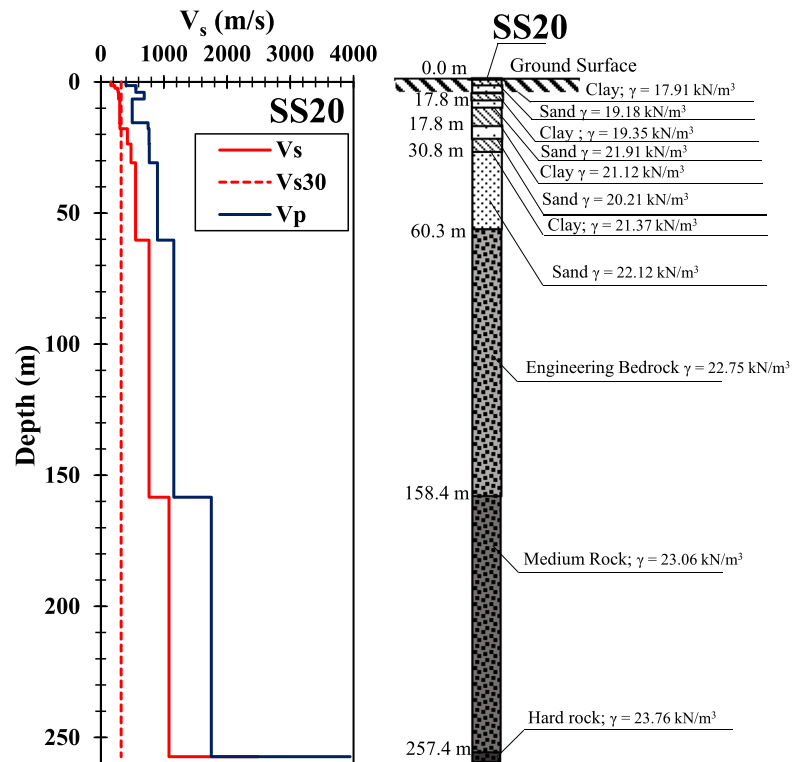
Based on the observation, it can be observed that among representative sites, TS35, located in the western part of

the study area, tends to have shallower bedrock. In line with the discussion on A_0 and f_0 , which was previously presented, the site with a larger A_0 and a smaller f_0 tends to have shallower bedrock. This seems reasonable and consistent with each other. Therefore, it could be concluded that the inversion analysis has approached actual conditions in the study area. In addition, sandy soils are generally dominant in the study area. Liquefaction could occur for sandy soils near the ground surface with a shallow groundwater level, especially for areas with high seismic vulnerability levels. Studies conducted by Stokoe et al. (1988) and Andrus et al. (2004) mentioned that sandy layers with V_s less than 180 m/s could be vulnerable to liquefaction. Mase et al. (2020), in the observation of liquefied sites in Northern Thailand, also mentioned that sand layers having low V_s are very vulnerable to undergoing liquefaction. Since the study area is located along the downstream area of the Muara Bangkahulu River, the groundwater

Fig. 10 V_p , V_s , V_{s30} , and soil profiles prediction from inversion analysis velocity and soil for sites SS1 (a), SS20 (b), SS24 (c), and TS35 (d)

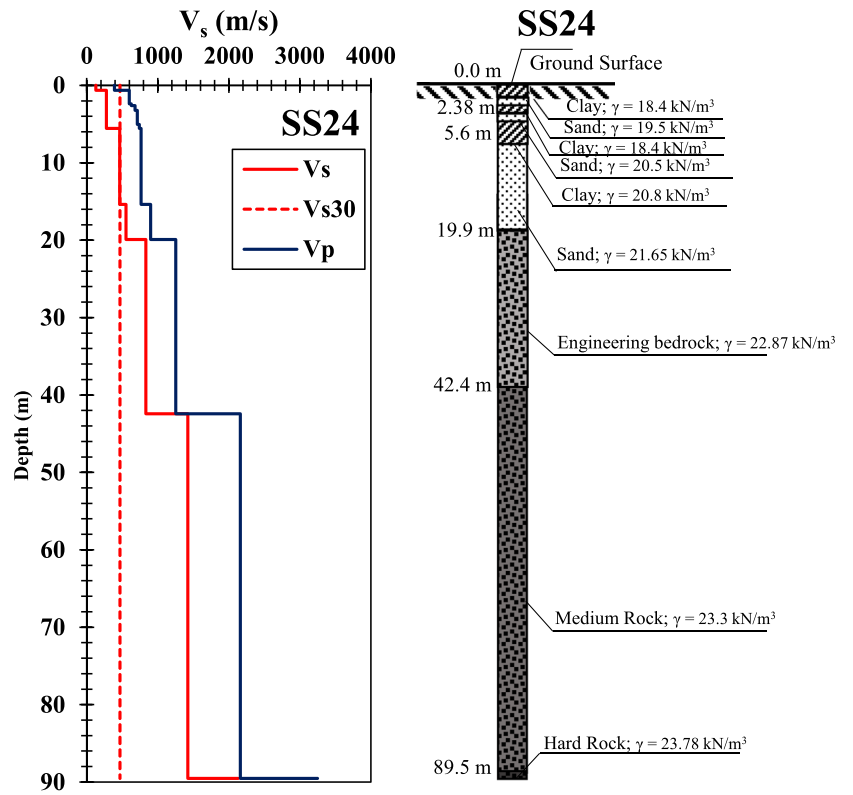


(a)

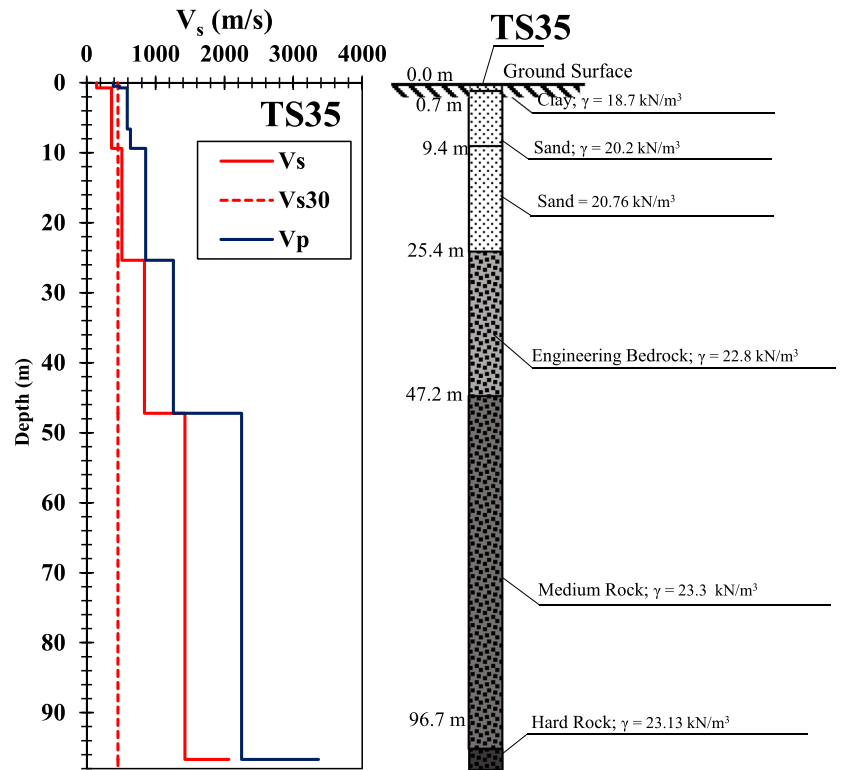


(b)

Fig. 10 (continued)



(c)



(d)

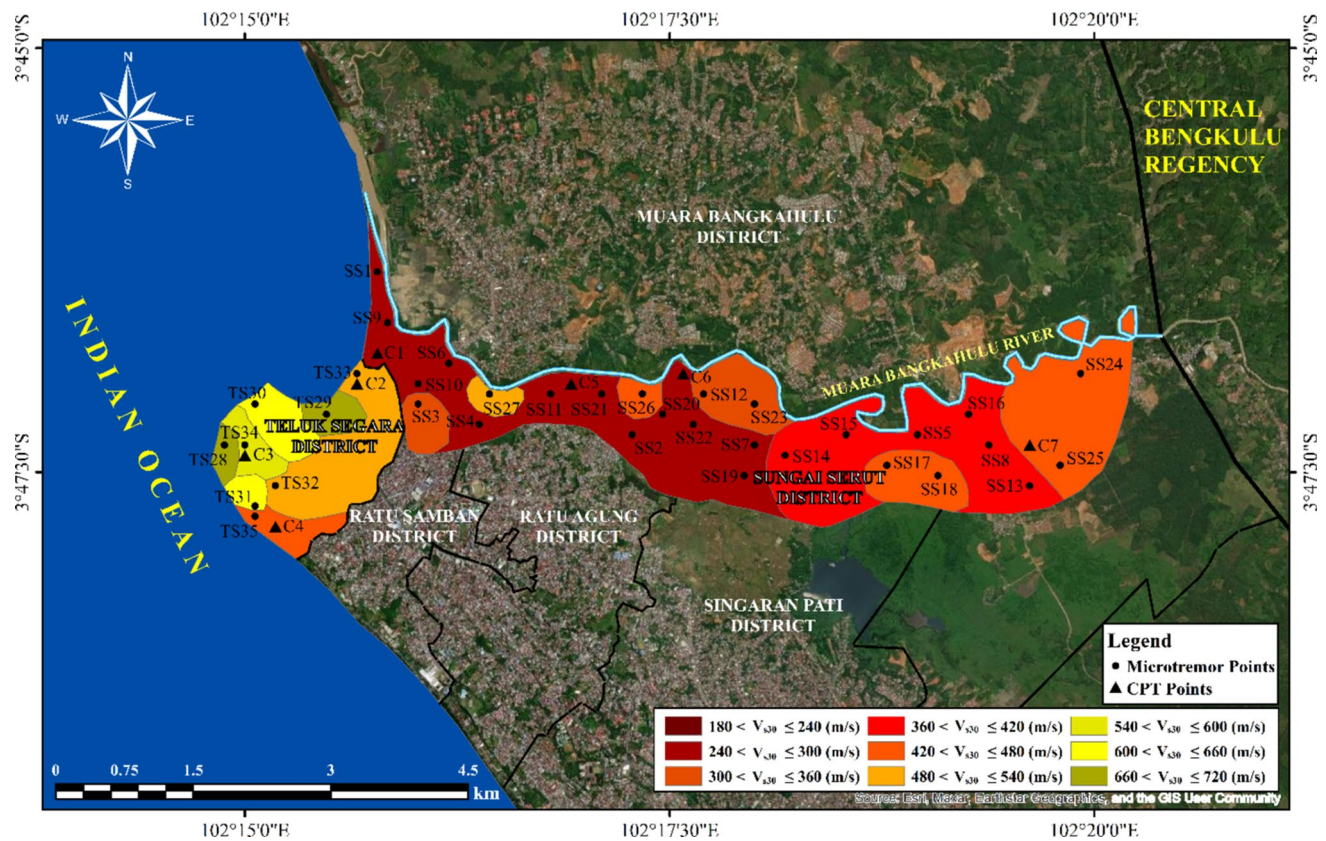


Fig. 11 Distribution map of V_{s30} in the study area

level is also relatively shallow. Therefore, the concern about soil damage should be the issue in the future.

V_{s30} and site class maps

Figure 11 presents a V_{s30} map for the study area. In Fig. 10, nine classes of V_{s30} are depicted for the study area. V_{s30} classes are namely 180–240 m/s; 240–300 m/s; 300–360 m/s; 360–420 m/s; 420–480 m/s; 480–540 m/s; 540–600 m/s; 600–660 m/s; and 660–720 m/s. The range is generally derived from NEHRP (1998). However, to observe a more detailed range, the V_{s30} from NEHRP is broken down every 60 m/s. This simplified procedure was adopted by several studies, such as Silva et al. (2015), Thompson and Wald (2012), and Cannon and Dutta (2015). It can be observed that there are three dominant ranges in the study area. The first one is V_{s30} of 180 to 240 m/s; the second one is V_{s30} of 420 to 480 m/s; and the third one is V_{s30} of 480 to 540 m/s. The first dominant range is generally found in the middle of the study area. The second and third dominant ranges are generally found in the eastern part of Bengkulu City. Based on the analysis, a further west, a larger V_{s30} . Therefore,

regarding soil resistance, sites located in the western part of Bengkulu City are generally larger.

The V_{s30} distribution generates the site class map, as presented in Fig. 12. Figure 12 shows that the study area is categorised as Class C and Class D. Class C is generally found in the middle to eastern parts of the study area and the western part. Class D is generally found in the middle of the study area’s northern part. According to site class distribution, the site class with low V_{s30} tends to have a higher risk of seismic impact. Wills et al. (2015) and Hollender et al. (2018) mentioned that those with lower V_{s30} could experience seismic impact due to the relatively lower soil density. During seismic loadings, such as earthquakes, the soil resistance is relatively lower than the site with higher V_{s30} . In line with K_g , very high seismic vulnerability is generally concentrated in Site Class D. Thitimakorn and Raenak (2016) also suggested that seismic impact for Site Class D in Northern Thailand is generally more significant than Site Class C. In line with this, Site Class D with very high K_g could undergo significant damage. Areas with this condition are generally located in the trading market area where several shops and housing exist. Therefore, implementing a seismic design code considering site conditions should be enforced in the study area.

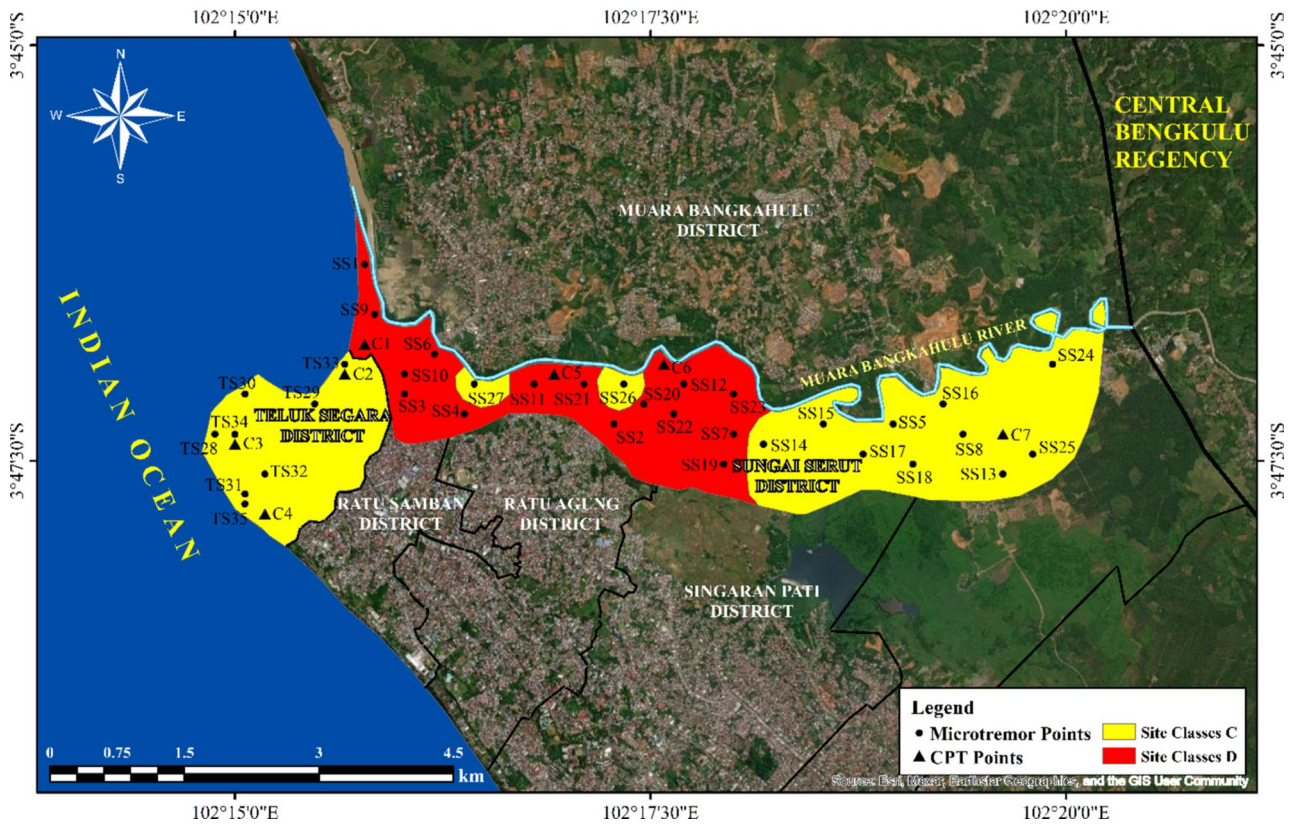


Fig. 12 Distribution map of Site Classes in the study area

Bedrock maps

Soft rock (engineering bedrock)

Figure 13 presents the study area's soft rock or engineering bedrock depth. The engineering bedrock surface is indicated by the minimum V_s of 760 m/s. From the figure, it can be observed that there are four zones of depth ranges for engineering bedrock in the study area. The ranges are 5–30 m; 30–55 m; 55–80 m; and 80–91 m. In general, the engineering bedrock depth in the study area is found at a depth of 5 to 33 m depth below the ground surface. This depth range is generally concentrated in the western part of the study area and from the middle to the eastern part of the study area. Another dominant range of engineering bedrock depth in the study area is the range of 30 to 55 m. This range is generally concentrated in the central part of the study area. The engineering bedrock depth range of 55 to 80 m is generally found in several small zones in the central part of the study area. The deepest engineering bedrock with a range of 80 to 91 m is generally found in a small part close to the estuary area.

Mase (2018) in the analysis of ground response analysis for the coastal area of Bengkulu City, assumed that the engineering bedrock surface is at a depth of 30 to 50 m. The assumption is generally consistent with the findings

presented in this study. Therefore, the map could be applicable for implementing seismic ground response in the study area. Several researchers, such as Adampira et al. (2015) and Qodri et al. (2021), also mentioned that the role of engineering bedrock could be crucial in seismic ground response analysis for ensuring the appropriate analysis.

Medium rock

The map of medium rock depth is presented in Fig. 14. In Fig. 14, it can be observed that there are four range zones for medium rock, namely 10–60 m; 60–110 m; 110–160 m, and 160–222.2 m. Based on the figure, there are two dominant ranges for medium rock depth in the study area. Medium bedrock with a depth of 10–60 m is generally found in the study area. This range is concentrated in the western part of the study area, the eastern part of the study area, and the middle part of the study area. For the 60–110 m range, the medium bedrock is generally found in the middle to the eastern part of the study area. A small zone of medium bedrock with a depth of 110–160 m is generally found in the middle of the study area. The deepest medium bedrock in the study area, with a range of 160–222.2 m, is generally found in the middle to the northwestern of the study area. In general, a further west, a shallower medium rock.

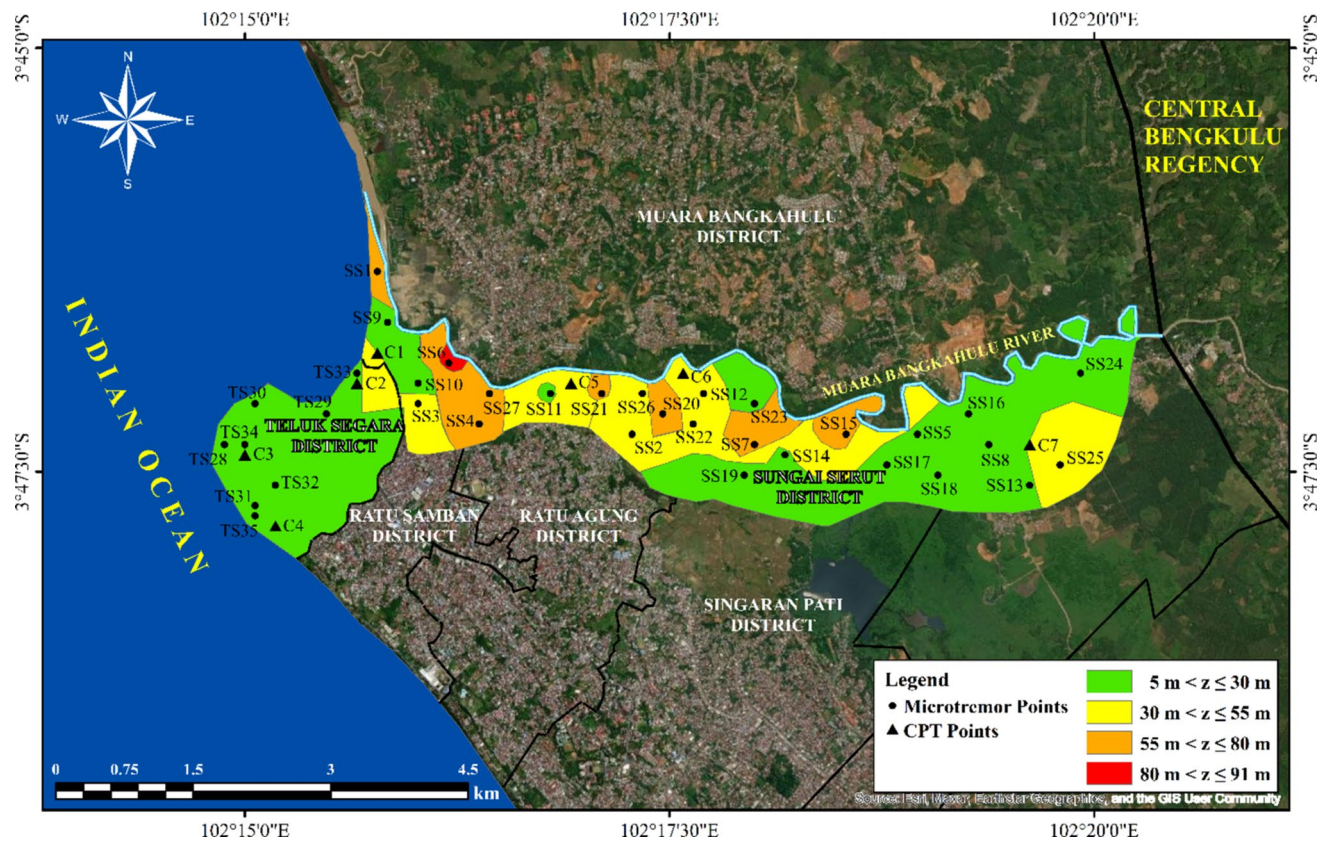


Fig. 13 Soft rock (engineering bedrock) map in the study area

The information on medium bedrock presented in this study can also be implemented in seismic ground response analysis. A study conducted by Chandran and Anbazhagan (2020) suggested the importance of bedrock surface information for ground response simulation. Using bedrock for elastic assumption in seismic ground response analysis is essential to ensure appropriate results (Likitlersuang et al. 2020). In line with these studies, the information on medium bedrock can be used for seismic ground response analysis in the study area.

Hard rock

Figure 15 presents the distribution map of hard rock or seismic bedrock in the study area. Hard rock is also grouped into four ranges, namely 40–100 m; 100–160 m; 160–220 m; and 220–289.2 m. In general, the seismic bedrock with depths ranging from 40 to 100 m is generally found in the study area. This depth range is concentrated in the western part of the study area, the middle to the eastern part. Another main depth range, namely 100–160 m, is found in the middle part of the study area to the eastern part of the study area. Bedrock depth ranging from 160 to 220 is generally found in small zones in the middle part of the study area and the base

of the estuary in the northwestern part. The deepest bedrock depth, with a range of 220 to 289.2 m, is generally found in the small zones in the middle part of the study area and the northwestern part of the study area. Overall, the further west, the shallower the seismic bedrock in the study area.

In line with engineering bedrock and medium rock, seismic bedrock is also important to understand. According to Yoshida (2015), seismic bedrock is important regardless of the structural engineering analysis for earthquake shaking simulation. For large-scale analysis, the seismic bedrock information could be helpful for future site response assessments, numerical modelling of seismic-wave propagation, dynamic ground response analyses, and site-specific seismic hazard evaluation at the basin scale Mascandola et al. (2023). Therefore, the bedrock maps and geophysical characteristics in the study area presented in this study can be implemented in further seismic ground response analysis research.

Consistency of bedrock depth based on previous studies

Studies conducted by Moon et al. (2019) and Manea et al. (2020) explained that bedrock depth in an area can be estimated based on empirical correlation related to site

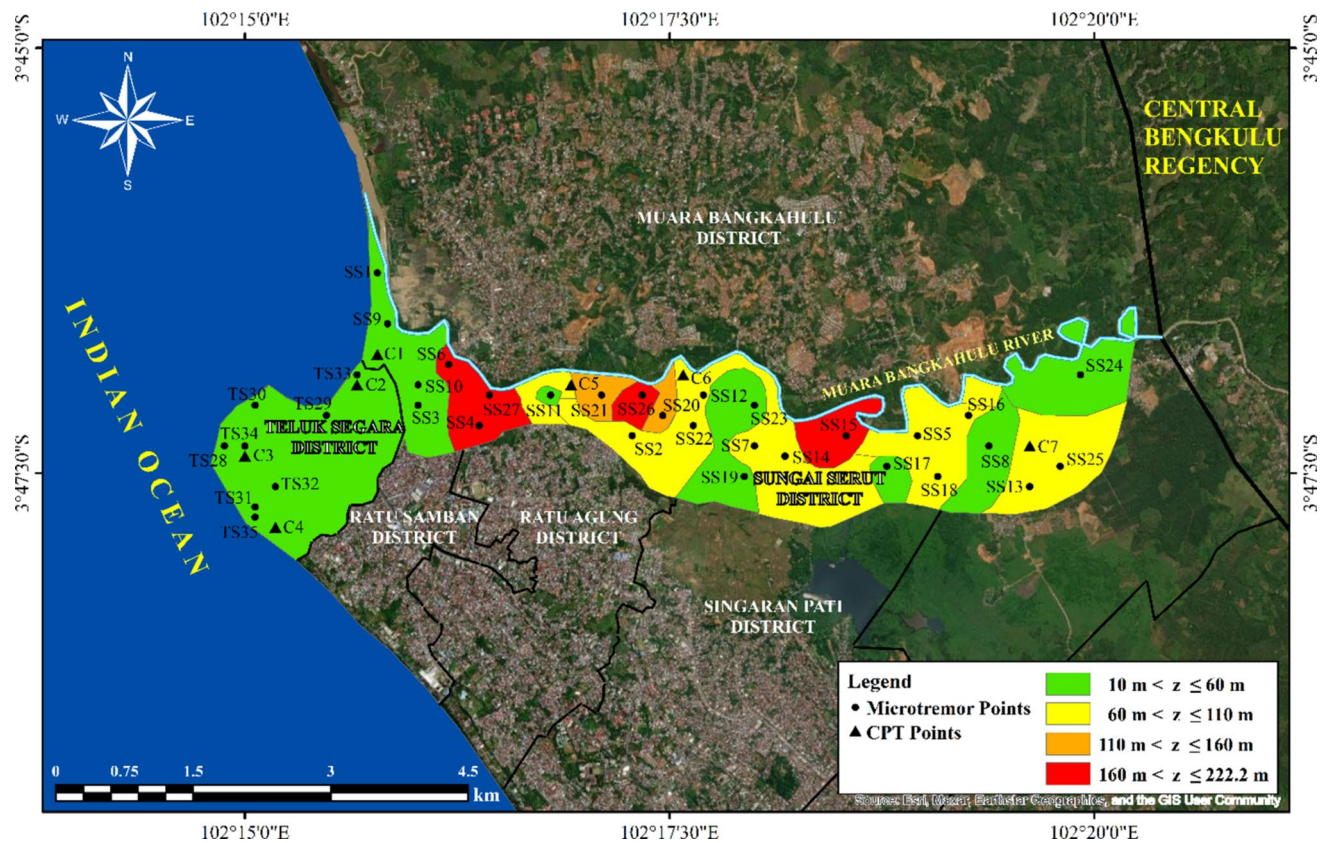


Fig. 14 Medium rock map in the study area

predominant frequency. Moon et al. (2019) suggested that the engineering bedrock depth can be estimated based on the following equation,

$$D = 92.5f^{-1.06} \tag{7}$$

In line with Moon et al. (2019), Manea et al. (2020) proposed an empirical equation to estimate bedrock depth as shown by the following equation

$$\log(D) = -1.18\log(f) + 5.01 \tag{8}$$

where D is the depth of engineering bedrock and f is the predominant frequency.

In this study, to check the consistency of estimated bedrock depths to the proposed estimations from previous studies, the bedrock depth proposed in this study is examined to measure the precision. Figures 16, 17 and 18 present the consistency of engineering bedrock to the empirical correlations from Moon et al. (2019) and Manea et al. (2020). For engineering bedrock, the consistency of engineering bedrock depth between the results and the prediction provided by Moon et al. (2019) and Manea et al. (2020) is shown in Figs. 16a and b. From the figures, it can be observed that the prediction of bedrock based on two approaches is generally

consistent with each other. The coefficients of determination (R^2) show values of 0.8366 and 0.8224. For medium rock (Fig. 16), the comparison is taken only based on Manea et al. (2020), since the formulation is addressed for all bedrock types. In Fig. 17, it can be observed that each estimated bedrock is generally consistent with the other. R^2 for data presented in Fig. 16 shows a value of 0.9187. In Fig. 18, the correlation for hard rock is also taken based on Manea et al. (2020). The comparison also exhibits consistency which is supported by an R^2 of 0.9075. In general, the results of this study are generally consistent with the previous studies. R^2 for the comparison is generally more than 0.75 which indicates that the tendency is consistent and the prediction is reliable. Therefore, based on comparisons, the bedrock depth based on frequency for this study is acceptable.

Model for bedrock depth prediction

The interpretation of bedrock depth for engineering practice is important to support other further analyses, such as seismic ground response analysis. In the future, geotechnical exploration to dig the subsoil information should be supported by the bedrock depth prediction. In this study, models to predict bedrock depth are proposed.

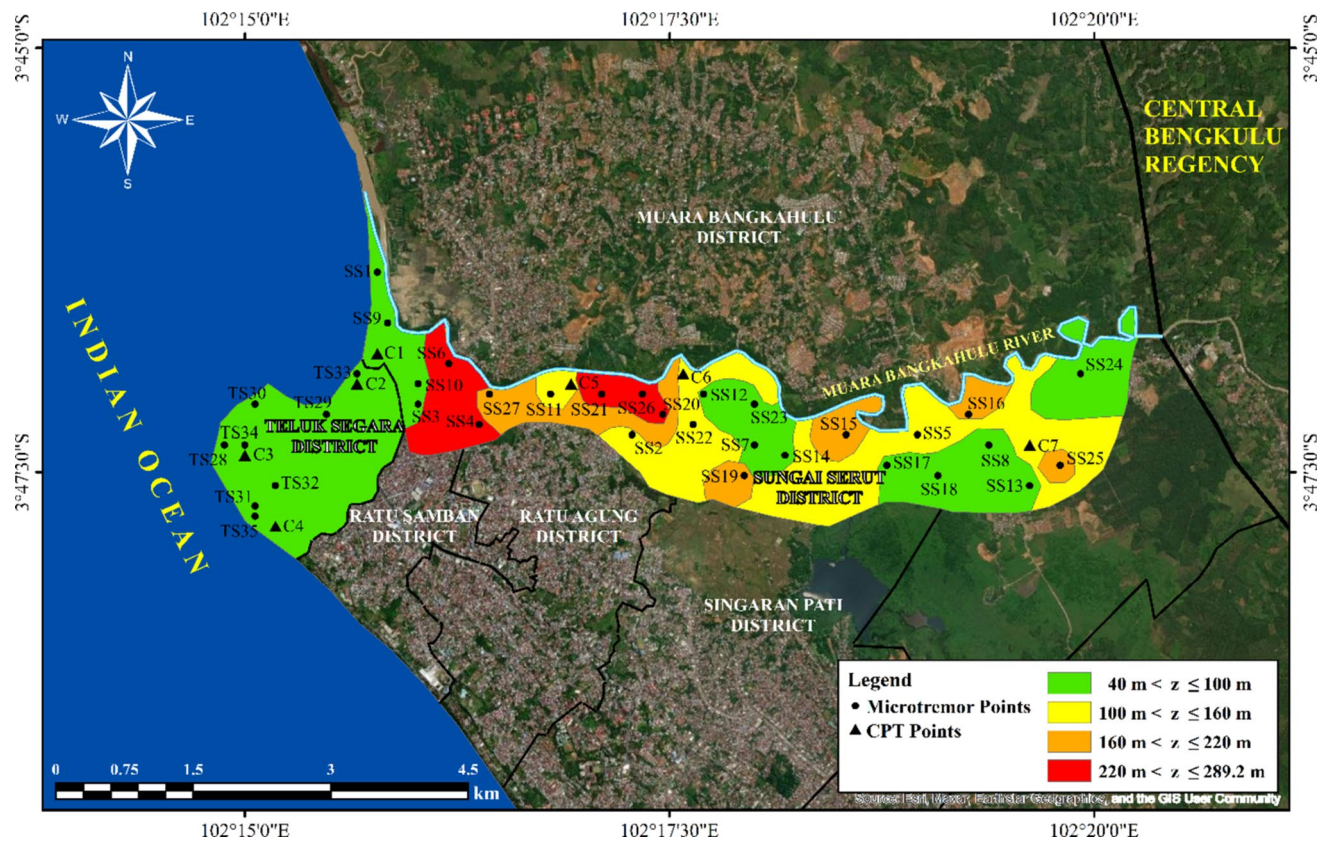


Fig. 15 Hard rock (seismic bedrock) map in the study area

Figure 19 presents the data analysis of bedrock depth corresponding to the predominant frequency for engineering bedrock (Fig. 19a), medium rock (Fig. 19b), and hard rock (Fig. 19c). Based on the figure, it can be observed that R^2 for the proposed models are generally larger than 0.75. It indicates that both bedrock depth and predominant frequency have a strong correlation. Based on the data analysis, the empirical equations for various bedrock types are proposed in the following equation

$$D = 52.968f_0^{-0.999}, \text{ with } R^2 \text{ of } 0.8494 \text{ for engineering bedrock} \tag{9}$$

$$D = 128.79f_0^{-0.617}, \text{ with } R^2 \text{ of } 0.8876 \text{ for medium rock} \tag{10}$$

$$D = 132.58f_0^{-0.546}, \text{ with } R^2 \text{ of } 0.8824 \text{ for hard rock} \tag{11}$$

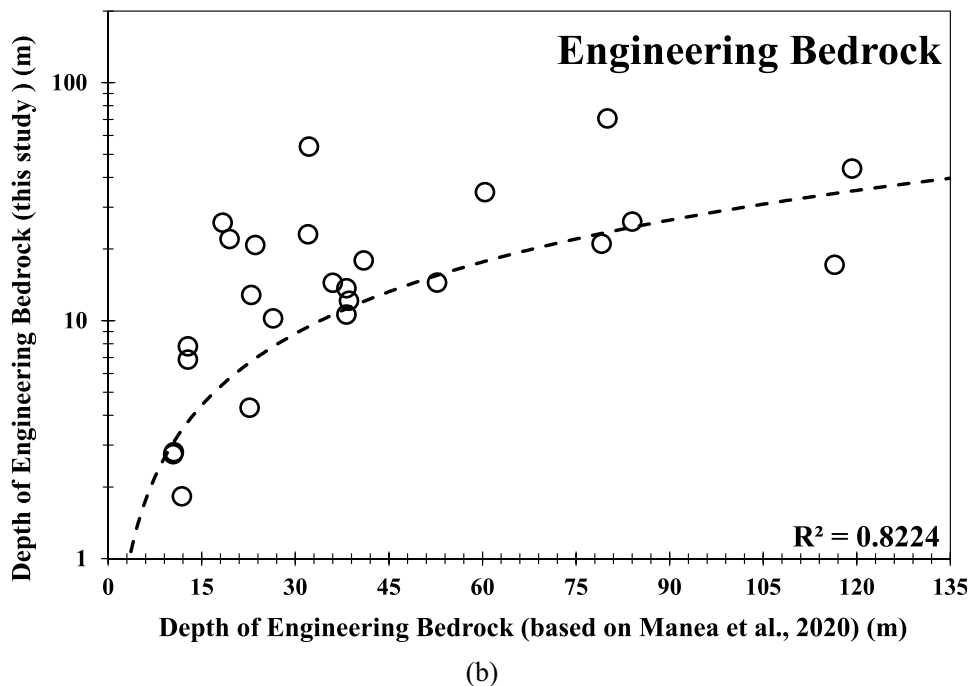
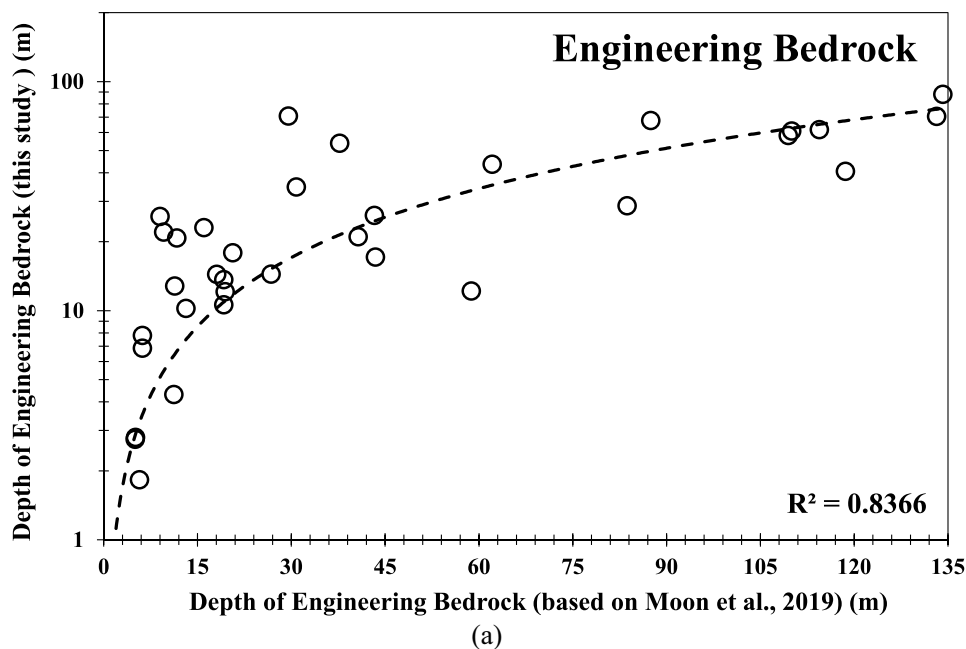
For practical implementation, Eqs. 9, 10 and 11 are used, and the results are depicted corresponding to predominant frequency for various depths, as presented in Fig. 20. Considering the performance and the consistency, the proposed graphs in Fig. 20 can be used for engineering practice, especially for seismic ground response analysis.

Model of ground profile

The one-dimensional ground profile obtained from the analysis generates three-dimensional and two-dimensional ground profiles, as presented in Fig. 21. In Fig. 21, cross-sections called Sections A-A (Fig. 21b) and B-B (Fig. 20c) are presented based on a three-dimensional ground profile (Fig. 21a). In general, there are six main layers underlain in the study area. The first is a thin clay layer, the second is a sand layer, the third is coarse sand and gravel, the fourth is engineering bedrock, the fifth is medium rock, and the last is hard rock. Figure 20 also shows that the study area tends to shape as a basin area, where the eastern and the western parts tend to have a shallower rock and in middle part tends to have a thicker sediment thickness. Several studies, as conducted by Korres et al. (2023), Mascandola et al. (2023), and Tsai et al. (2021), mentioned that the basin effect could influence the characteristic of seismic response in an area. Therefore, the role of basin geological conditions should be carefully understood. The implication on the basin could relate to seismic hazard assessment and seismic resistance design in the investigated area.

Nakamura (1989) suggested that soft soil sediment and the impedance contrast between sediment and bedrock are

Fig. 16 Consistency of engineering bedrock depth based on Moon et al. (2019) (a) and Manea et al. (2020) (b)



significantly correlated. Ground profiles with a lower f_0 can potentially have soft soil sediment thickness (Mase et al. 2021a). A soil layer with lower frequency (greater layer thickness) can also produce smaller surface response spectra, especially at short periods and vice versa (Likitlersuang et al. 2020; Misliniyati et al. 2019). Anbazhagan et al. (2013) revealed a higher spectral acceleration and amplification at short periods for the sites with shallow bedrock. In general, the ground profile from this study

can be used to perform a two-dimensional or three-dimensional seismic response analysis in the study area.

Concluding remarks

Several concluding remarks from this study can be drawn in the following points,

Fig. 17 Consistency of medium rock depth based on Manea et al. (2020)

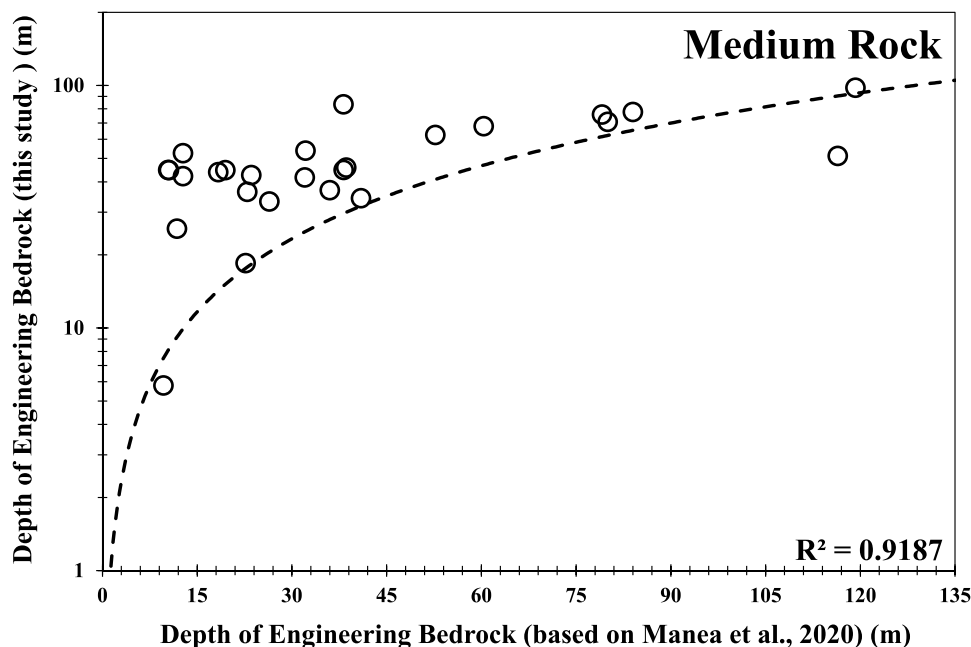
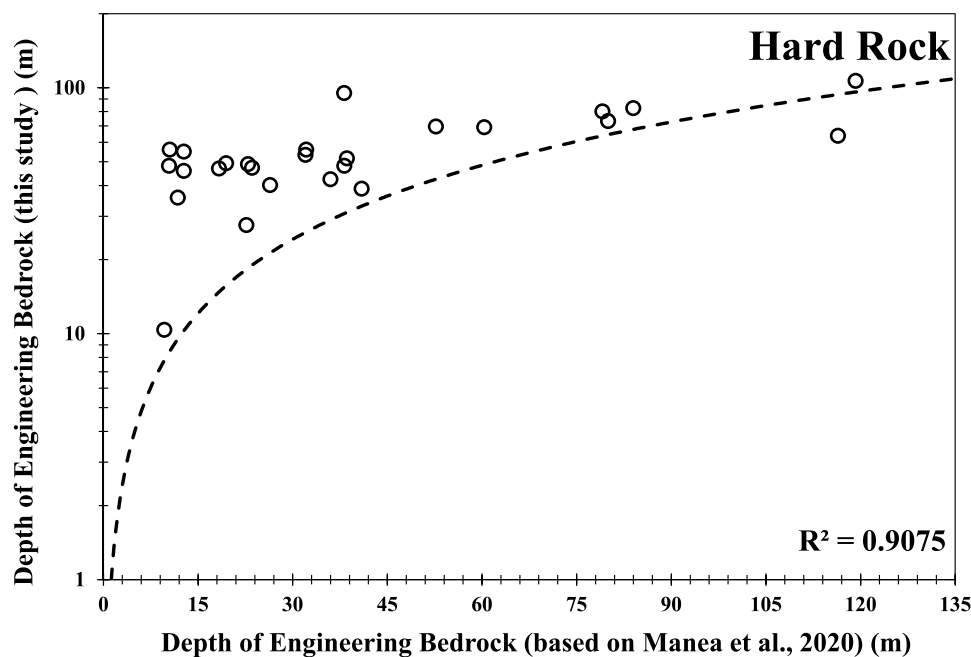


Fig. 18 Consistency of hard rock depth based on Manea et al. (2020)



1. A larger vulnerability level is found in areas having low V_{s30} and Site Class D, which is very susceptible to undergoing more significant seismic impact. It is unique that the basin of the study area is dominated by Site Class D, whereas the eastern and western parts of the study area are dominated by Site Class C. The basin area especially trading market areas and the estuary of the river tends to have very high seismic vulnerability. Since there is a variation of land use in the study area, seismic hazard mitigation should be considered, espe-

cially during construction planning and before construction. Therefore, the concern of seismic hazard mitigation should be enforced. The results are also applicable as preliminary guidelines to update spatial plans in the study area.

2. Bedrock maps proposed in this study are very useful for preliminary information before conducting a site investigation. The bedrock information is also useful for simulating seismic ground response analysis. Therefore, the maps can be used for further study. Besides, the seismic

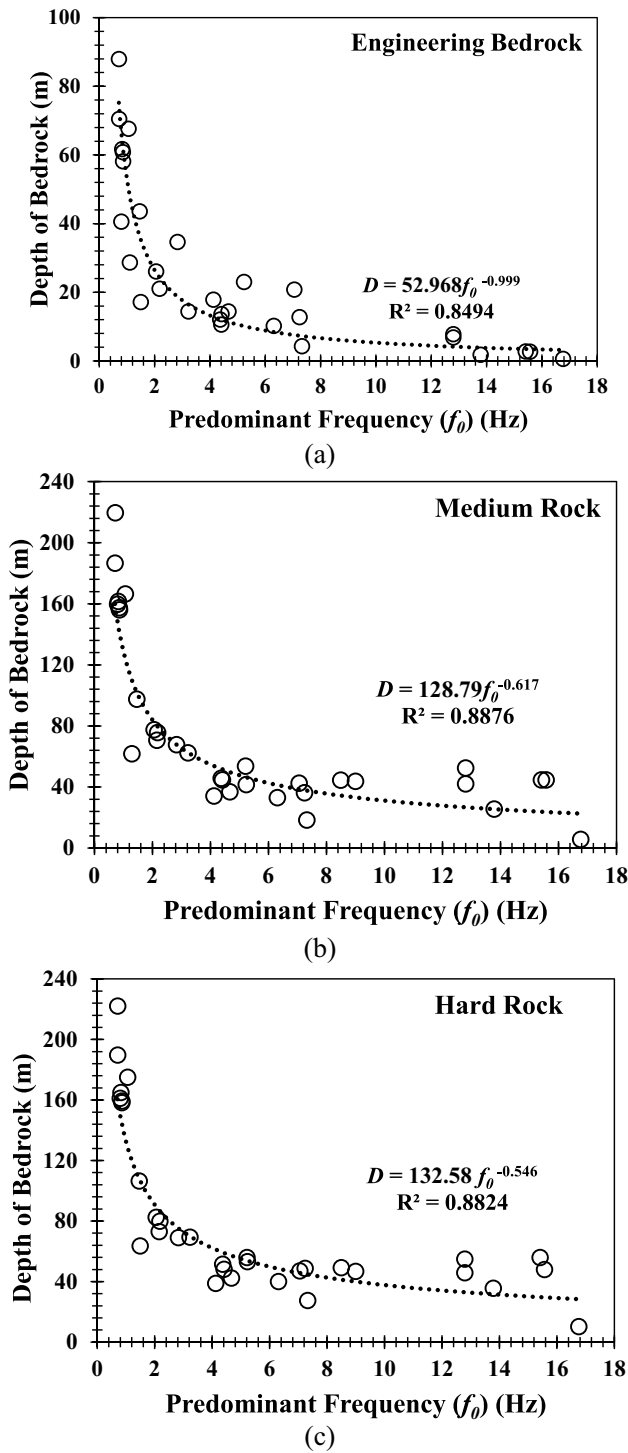


Fig. 19 Tendency of depth of bedrock and predominant frequency for various bedrock types: engineering bedrock (a), medium rock (b), and hard rock (c)

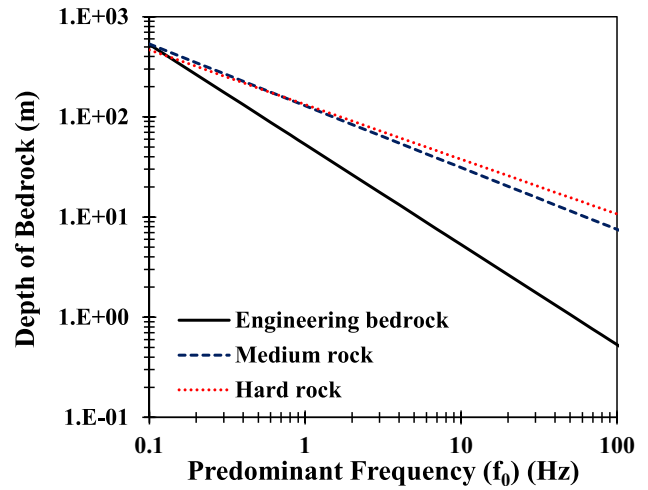
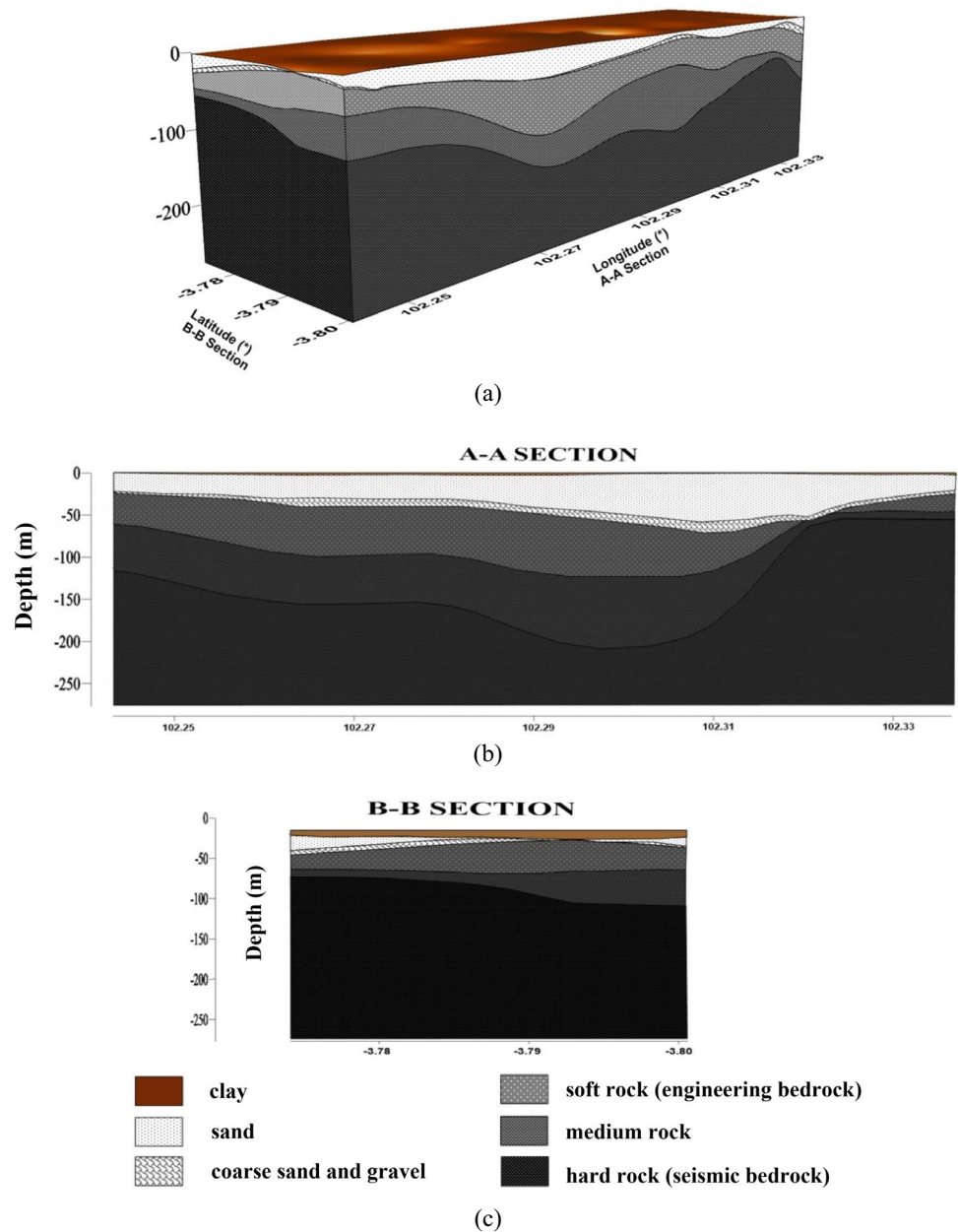


Fig. 20 Proposed graphs to predict bedrock depth in the study area

ground response analysis based on either deterministic or probabilistic seismic hazard analysis could be used to develop a seismic hazard map. The information is further used as the consideration for construction design in the study area. The three-dimensional geological modelling developed in this study could be implemented for further study.

3. The prediction of bedrock depths presented in this study is generally consistent with previous studies. The bedrock depth has a good correlation with the predominant frequency. Therefore, the prediction of bedrock in this study is acceptable. The empirical models proposed in this study are reliable and can be implemented for another analysis, such as seismic ground response analysis.
4. The subsoil profile in three-dimensional form shows that the tendency of the ground profile in the study area is shaped as a basin. It is shown that shallow bedrock in the eastern and western parts is relatively shallow. In line with the seismic vulnerability prediction, the basin area has a high seismic vulnerability with low soil resistance. The area is also now developed as the market zone where the most centralised population in the study area exists. The dense population in high-seismic vulnerability zones should be concerned. The characteristics of the basin and its possible effect on seismic damage should be also carefully considered. A local seismic design code for the study area should be proposed. It will be presented in further study.

Fig. 21 Ground profile of the downstream area of the Muara Bangkahulu River: 3D subsoil profile (a), 2D profile for A-A Section (b), and 2D profile for B-B Section (c)



Acknowledgements The authors would like to thank the Research Institutions and Community Services, University of Bengkulu, for financial support on the professor acceleration research 2023 with contract reference no. 2132/UN30.15/PP/2023. This study is also partially supported by the Visiting Researcher Batch 3 program from the National Research and Innovation Agency (BRIN), Indonesia, with contract reference no. 15/II/HK/2023. The work was performed under the Japan-ASEAN Science and Technology Innovation Platform (JASTIP-WP4).

Author contribution • Lindung Zalbuin Mase: conceptualization, writing-original draft, methodology, data analysis, visualization, review—editing, project administration

- Masyhur Irsyam: conceptualization, methodology, data analysis, visualization, review—editing
- Dian Gustiparani: data analysis, writing-original draft, visualization
- Annisa Nur Noptapia: data analysis, visualization
- Arifan Jaya Syahbana: conceptualization, data analysis, review—editing
- Eko Soebowo: conceptualization, review—editing

Data availability All the datasets used and analysed during the current study are available from the corresponding author at the reasonable request.

Declarations

Conflict of interest The authors declare no competing interests.

References

- Adampira M, Alielahi H, Panji M, Koohsari H (2015) Comparison of equivalent linear and nonlinear methods in seismic analysis of liquefiable site response due to near-fault incident waves: a case study. *Arab J Geosci* 8:3103–3118. <https://doi.org/10.1007/s12517-014-1399-6>
- Ahdi, S. K., Kwak, D. Y., Ancheta, T. D., Contreras, V., Kishida, T., Kwok, A. O., ... & Stewart, J. P. (2022). Site parameters applied in NGA-Sub database. *Earthquake Spectra*, 38(1), 494–520. <https://doi.org/10.1177/87552930211043536>
- Akkaya İ (2020) Availability of seismic vulnerability index (K_g) in the assessment of building damage in Van, Eastern Turkey. *Earthq Eng Vib* 19:189–204. <https://doi.org/10.1007/s11803-020-0556-z>
- Andrus RD, Stokoe KH, Hsein Juang C (2004) Guide for shear-wave-based liquefaction potential evaluation. *Earthq Spectra* 20(2):285–308. <https://doi.org/10.1193/1.1715106>
- Baise LG, Kaklamanos J, Berry BM, Thompson EM (2016) Soil amplification with a strong impedance contrast: Boston, Massachusetts. *Eng Geol* 202:1–13. <https://doi.org/10.1016/j.enggeo.2015.12.016>
- Cannon, E. C., & Dutta, U. (2015). Evaluating topographically-derived V_{s30} values for seismic site class characterization in Anchorage, Alaska, USA. In *Proceeding of the 6th International Conference on Earthquake Geotechnical Engineering*, Christchurch, 1- 4 November 2015, New Zealand.
- Chandran D, Anbazhagan P (2020) 2D nonlinear site response analysis of typical stiff and soft soil sites at shallow bedrock regions with low to medium seismicity. *J Appl Geophys* 179:104087. <https://doi.org/10.1016/j.jappgeo.2020.104087>
- Farazi AH, Hossain MS, Ito Y, Piña-Flores J, Kamal AM, Rahman MZ (2023) Shear wave velocity estimation in the Bengal Basin, Bangladesh by HVSR analysis: implications for engineering bedrock depth. *J Appl Geophys* 211:104967. <https://doi.org/10.1016/j.jappgeo.2023.104967>
- Fat-Helbary RES, El-Faragawy KO, Hamed A (2019) Application of HVSR technique in the site effects estimation at the south of Marsa Alam city, Egypt. *Journal of African Earth Sciences* 154:89–100. <https://doi.org/10.1016/j.jafrearsci.2019.03.015>
- García-Jerez A, Piña-Flores J, Sánchez-Sesma FJ, Luzón F, Pertón M (2016) A computer code for forward calculation and inversion of the H/V spectral ratio under the diffuse field assumption. *Comput Geosci* 97:67–78. <https://doi.org/10.1016/j.cageo.2016.06.016>
- Gosar A (2017) Study on the applicability of the microtremor HVSR method to support seismic microzonation in the town of Idrija (W Slovenia). *Nat Hazard* 17(6):925–937. <https://doi.org/10.5194/nhess-17-925-2017>
- Herak M (2008) ModelHVSR—a Matlab® tool to model the horizontal-to-vertical spectral ratio of ambient noise. *Comput Geosci* 34(11):1514–1526. <https://doi.org/10.1016/j.cageo.2007.07.009>
- Hollender, F., Cornou, C., Dechamp, A., Oghalaei, K., Renalier, F., Maufroy, E., ... & Sicilia, D. (2018). Characterization of site conditions (soil class, VS30, velocity profiles) for 33 stations from the French permanent accelerometric network (RAP) using surface-wave methods. *Bulletin of Earthquake Engineering*, 6(6), 2337–2365. <https://doi.org/10.1007/s10518-017-0135-5>
- Imai T, Tonouchi K (1982) Correlation of N-value with S-wave velocity and shear modulus. In: *Proc. 2nd European Symp. Of Penetration Testing*. Amsterdam, pp 57–72
- Kanai K (1983) *Engineering seismology*. University of Tokyo Press, Tokyo
- Koçkar MK, Akgün H (2012) Evaluation of the site effects of the Ankara basin, Turkey. *J Appl Geophys* 83:120–134. <https://doi.org/10.1785/BSSA0860061692>
- Korres, M., Lopez-Caballero, F., Alves Fernandes, V., Gatti, F., Zentner, I., Voldoire, F., ... & Castro-Cruz, D. (2023). Enhanced seismic response prediction of critical structures via 3D regional scale physics-based earthquake simulation. *Journal of earthquake engineering*, 27(3), 546–574. <https://doi.org/10.1080/13632469.2021.2009061>
- Kumar A, Satyannarayana R, Rajesh BG (2022) Correlation between SPT-N and shear wave velocity (V_g) and seismic site classification for Amaravati city. *India Journal of Applied Geophysics* 205:104757. <https://doi.org/10.1016/j.jappgeo.2022.104757>
- Kurnio H, Fekete A, Naz F, Norf C, Jüpner R (2021) Resilience learning and indigenous knowledge of earthquake risk in Indonesia. *Int J Disaster Risk Reduct* 62:102423. <https://doi.org/10.1016/j.ijdrr.2021.102423>
- Lachet, C., Hatzfeld, D., Bard, P. Y., Theodulidis, N., Papaioannou, C., & Savvaïdis, A. (1996) Site effects and microzonation in the city of Thessaloniki (Greece) comparison of different approaches 86 (6), 1692–1703. <https://doi.org/10.1785/BSSA0860061692>
- Likitlersuang S, Plengsiri P, Mase LZ, Tanapalungkorn W (2020) Influence of spatial variability of ground on seismic response analysis: a case study of Bangkok subsoils. *Bull Eng Geol Env* 79(1):39–51. <https://doi.org/10.1007/s10064-019-01560-9>
- Manea EF, Cioflan CO, Coman A et al (2020) Estimating geophysical bedrock depth using single station analysis and geophysical data in the extra-carpathian area of Romania. *Pure Appl Geophys* 177:4829–4844. <https://doi.org/10.1007/s00024-020-02548-3>
- Martorana R, Capizzi P, D'Alessandro A, Luzio D, Di Stefano P, Renda P, Zarcone G (2018) Contribution of HVSR measures for seismic microzonation studies. *Ann Geophys*. <https://doi.org/10.4401/ag-7786>
- Mascandola C, Barani S, Albarello D (2023) Impact of site-response characterization on probabilistic seismic hazard in the Po plain (Italy). *Bull Seismol Soc Am*. <https://doi.org/10.1785/0120220177>
- Mase LZ (2018) Reliability study of spectral acceleration designs against earthquakes in Bengkulu City Indonesia. *Int J Technol* 9(5):910–924. <https://doi.org/10.14716/ijtech.v9i5.621>
- Mase LZ, Keawsawasvong S (2022) Seismic hazard maps of Bengkulu City, Indonesia, considering probabilistic spectral response for medium and stiff soils. *Open Civ Eng J* 16(1):e187414952210210. <https://doi.org/10.2174/18741495-v16-e221021-2022-49>
- Mase LZ, Sugianto N, Refrizon (2021a) Seismic hazard microzonation of Bengkulu City, Indonesia. *Geoenviron Disaster* 8:1–17. <https://doi.org/10.1186/s40677-021-00178-y>
- Mase LZ, Likitlersuang S, Tobita T, Chairprakaikeow S, Soralump S (2020) Local site investigation of liquefied soils caused by earthquake in Northern Thailand. *J Earthquake Eng* 24(7):1181–1204. <https://doi.org/10.1080/13632469.2018.1469441>
- Mase LZ, Refrizon R et al (2021b) Local site investigation and ground response analysis on downstream area of Muara Bangkahulu River, Bengkulu City, Indonesia. *Indian Geotech J* 51:952–966. <https://doi.org/10.1007/s40098-020-00480-w>
- Mase LZ, Likitlersuang S, Tobita T (2022) Verification of liquefaction potential during the strong earthquake at the border of Thailand-Myanmar. *J Earthquake Eng* 26(4):2023–2050. <https://doi.org/10.1080/13632469.2020.1751346>
- Mase LZ, Agustina S, Hardiansyah et al (2023b) Application of simplified energy concept for liquefaction prediction in Bengkulu City, Indonesia. *Geotech Geol Eng* 41:1999–2021. <https://doi.org/10.1007/s10706-023-02388-7>
- Mase, L. Z., Wahyuni, M. S., Hardiansyah, & Syahbana, A. J. (2023a). Prediction of damage intensity level distribution in Bengkulu City, during the Mw 8.6 Bengkulu-Mentawai Earthquake in 2007,

- Indonesia. Transportation Infrastructure Geotechnology, 1–25. <https://doi.org/10.1007/s40515-023-00306-1>
- Mase LZ, Amri, K, Ueda K, Apriani R, Utami F, Tobita T, Likitlersuang S (2023c) Geophysical investigation on the subsoil characteristics of the Dendam Tak Sudah Lake site in Bengkulu City, Indonesia. *Acta Geophysica*. (minor revision). <https://doi.org/10.1007/s11600-023-01158-6>
- McGann CR, Bradley BA, Taylor ML, Wotherspoon LM, Cubrinovski M (2015) Development of an empirical correlation for predicting shear wave velocity of Christchurch soils from cone penetration test data. *Soil Dyn Earthq Eng* 75:66–75. <https://doi.org/10.1016/j.soildyn.2015.03.023>
- Miller RD, Xia J, Park CB, Ivanov J, Williams E (1999) Using MASW to map bedrock in Olathe, Kansas. In: SEG Technical Program Expanded Abstracts 1999. Society of Exploration Geophysicists, pp 433–436. <https://doi.org/10.1190/1.1821045>
- Mirzaoglu M, Dykmen U (2003) Application of microtremor to seismic microzoning procedure. *J Balkan Geophys Soc* 6(3):143–156
- Misliniyati R, Mase LZ, Irsyam M, Hendriawan H, Sahadewa A (2019) Seismic response validation of simulated soil models to vertical array record during a strong earthquake. *J Eng Technol Sci* 51(6):772–790. <https://doi.org/10.5614/j.eng.technol.sci.2019.51.6.3>
- Misliniyati, R., Mase, L. Z., Syahbana, A. J., & Soebowo, E. (2018, December). Seismic hazard mitigation for Bengkulu Coastal area based on site class analysis. In IOP Conference Series: Earth and Environmental Science (Vol. 212, No. 1, p. 012004). IOP Publishing. <https://doi.org/10.1088/1755-1315/212/1/012004>
- Molnar S, Cassidy JF, Castellaro S et al (2018) Application of microtremor horizontal-to-vertical spectral ratio (MHVSR) analysis for site characterization: state of the art. *Surv Geophys* 39:613–631. <https://doi.org/10.1007/s10712-018-9464-4>
- Moon SW, Subramaniam P, Zhang Y, Vinoth G, Ku T (2019) Bedrock depth evaluation using microtremor measurement: empirical guidelines at weathered granite formation in Singapore. *J Appl Geophys* 171:103866. <https://doi.org/10.1016/j.jappgeo.2019.103866>
- Nakamura Y (1989) A method for dynamic characteristic estimation of subsurface using microtremor on ground surface. *Q Rep Railw Tech Res* 30(1):25–53
- Nakamura Y (2008) “On the H/V spectrum,” the 14th world conference on earthquake engineering, October 12–17. Beijing, China
- National Earthquake Hazards Reduction Program (NEHRP) (1998) Recommended provisions for seismic regulation for new buildings and other structures: part 1-provisions and part 2-commentary, FEMA 302. Texas, USA
- Okada H, Suto K (2003) The microtremor survey method. Society of Exploration Geophysicists. <https://doi.org/10.1190/1.9781560801740>
- Pinzón LA, Pujades LG, Macau A, Carreño E, Alcalde JM (2019) Seismic site classification from the horizontal-to-vertical response spectral ratios: use of the Spanish strong-motion database. *Geosciences* 9(7):294. <https://doi.org/10.3390/geosciences9070294>
- Putrie, N. S., Susiloningtyas, D., & Pratami, M. (2019, May). Distribution pattern of Settlement in 2032 based on population density in Bengkulu City. In IOP Conference Series: Earth and Environmental Science (Vol. 284, No. 1, p. 012007). IOP Publishing. <https://doi.org/10.1088/1755-1315/284/1/012007>
- Putti SP, Satyam N (2020) Evaluation of site effects using HVSR microtremor measurements in Vishakhapatnam (India). *Earth Syst Environ* 4:439–454. <https://doi.org/10.1007/s41748-020-00158-6>
- Qodri MF, Mase LZ, Likitlersuang S (2021) Non-linear site response analysis of Bangkok subsoils due to earthquakes triggered by Three Pagodas Fault. *Eng J* 25(1):43–52. <https://doi.org/10.4186/ej.2021.25.1.43>
- Sadeghi SH, Gharemahmudli S, Kheirfam H, Darvishan AK, Harchegani MK, Saeidi P, Vafakhah M (2018) Effects of type, level and time of sand and gravel mining on particle size distributions of suspended sediment. *Int Soil Water Conserv Res* 6(2):184–193. <https://doi.org/10.1016/j.iswcr.2018.01.005>
- Salencon J (2001) Handbook of Continuum Mechanics: General Concepts. Thermoelasticity Springer Science and Business Media, Berlin, Germany
- SESAME (2004) Guidelines for the implementation of the H/V spectral ratio technique on ambient vibrations measurements, processing and interpretation. SESAME European research project, Deliverable D23. 12., Project No. EVG1-CT-2000-00026 SESAME, p 62
- Silva V, Crowley H, Varum H, Pinho R (2015) Seismic risk assessment for mainland Portugal. *Bull Earthq Eng* 13:429–457. <https://doi.org/10.1007/s10518-014-9630-0>
- Stanko D, Markušić S (2020) An empirical relationship between resonance frequency, bedrock depth and V_{S30} for Croatia based on HVSR forward modelling. *Nat Hazards* 103(3):3715–3743. <https://doi.org/10.1007/s11069-020-04152-z>
- Stokoe KH, Roesset JM, Bierschwale JG, Aouad M (1988) Liquefaction potential of sands from shear wave velocity. *Proc of the 9th world conference on earthquake engineering* 3 (1):213–218.
- Sukkarak R, Tanapalungkorn W, Likitlersuang S, Ueda K (2021) Liquefaction analysis of sandy soil during strong earthquake in Northern Thailand. *Soils Found* 61(5):1302–1318. <https://doi.org/10.1016/j.sandf.2021.07.003>
- Tanapalungkorn W, Mase LZ, Latcharote P, Likitlersuang S (2020) Verification of attenuation models based on strong ground motion data in Northern Thailand. *Soil Dyn Earthq Eng* 133:106145. <https://doi.org/10.1016/j.soildyn.2020.106145>
- Thitimakorn T, Raenak T (2016) NEHRP site classification and preliminary soil amplification maps of Lamphun City, Northern Thailand. *Open Geosci* 8(1):538–547. <https://doi.org/10.1515/geo-2016-0046>
- Thompson EM, Wald DJ (2012) Developing V_{S30} site-condition maps by combining observations with geologic and topographic constraints. In: Proceeding of 15th World conference on earthquake engineering, Lisboa, Portugal
- Tian B, Du Y, Jiang H, Zhang R, Zhang J (2020) Estimating the shear wave velocity structure above the fresh bedrock based on small scale microtremor observation array. *Bull Eng Geol Env* 79:2997–3006. <https://doi.org/10.1007/s10064-020-01761-7>
- Tsai CC, Kishida T, Lin WC (2021) Adjustment of site factors for basin effects from site response analysis and deep downhole array measurements in Taipei. *Eng Geol* 285:106071. <https://doi.org/10.1016/j.enggeo.2021.106071>
- Wathelet M (2008) An improved neighborhood algorithm: parameter conditions and dynamic scaling. *Geophys Res Lett* 35(9):L09301. <https://doi.org/10.1029/2008GL033256>
- Wills CJ, Gutierrez CI, Perez FG, Branum DM (2015) A next generation V_{S30} map for California based on geology and topography. *Bull Seismol Soc Am* 105(6):3083–3091. <https://doi.org/10.1785/0120150105>